Quasi-static Eocene–Oligocene climate in Patagonia promotes slow faunal evolution and mid-Cenozoic global cooling

CrossMark

Matthew J. Kohn [a,*], Caroline A.E. Strömberg [b], Richard H. Madden [c], Regan E. Dunn [b], Samantha Evans [a], Alma Palacios [a], Alfredo A. Carlini [d]

[a] Department of Geosciences, Boise State University, Boise, ID 83725, USA
[b] Department of Biology and Burke Museum of Natural History and Culture, University of Washington, Seattle, WA 98195, USA
[c] Department of Organismal Biology and Anatomy, University of Chicago, Chicago, IL 60637, USA
[d] Departamento de Paleontología de Vertebrados, Universidad Nacional de La Plata (CONICET), La Plata B1900FWA, Argentina

ARTICLE INFO

ABSTRACT

New local/regional climatic data were compared with floral and faunal records from central Patagonia to investigate how faunas evolve in the context of local and global climates. Oxygen isotope compositions of mammal fossils between c. 43 and 21 Ma suggest a nearly constant mean annual temperature of 16 ± 3 °C, consistent with leaf physiognomic and sea surface studies that imply temperatures of 16–18 °C. Carbon isotopes in tooth enamel track atmospheric δ^{13}C, but with a positive deviation at 27.2 Ma, and a strong negative deviation at 21 Ma. Combined with paleosol characteristics and reconstructed Leaf Area Indices (rLAIs), these trends suggest aridification from 45 Ma (c. 1200 mm/yr) to 43 Ma (c. 450 mm/yr), quasi-constant MAP until at least 31 Ma, and an increase to ~800 mm/yr by 21 Ma. Comparable MAP through most of the sequence is consistent with relatively constant floral compositions, rLAI, and leaf physiognomy. Abundance of palms reflects relatively dry-adapted lineages and greater drought tolerance under higher p_{CO2}. Pedogenic carbonate isotopes imply low $p_{CO2} = 430 \pm 300$ ppmv at the initiation of the Eocene–Oligocene climatic transition. Arid conditions in Patagonia during the late Eocene through Oligocene provided dust to the Southern Ocean, enhancing productivity of silicifiers, drawdown of atmospheric CO$_2$, and protracted global cooling. As the Antarctic Circumpolar Current formed and Earth cooled, wind speeds increased across Patagonia, providing more dust in a positive climate feedback. High tooth crowns (hypsodonty) and ever-growing teeth (hypselodonty) in notoungulates evolved slowly and progressively over 20 Ma after initiation of relatively dry environments through natural selection in response to dust ingestion. A Ratchet evolutionary model may explain protracted evolution of hypsodonty, in which small variations in climate or dust delivery in an otherwise static environment drive small morphological shifts that accumulate slowly over geologic time.

© 2015 Elsevier B.V. All rights reserved.

1. Introduction

Patagonian strata of South America encode a remarkable record of climate, ecology, and faunal evolution spanning much of the Cenozoic. Most spectacularly, South American notoungulates and other herbivorous lineages show a pattern of increasing cheek tooth crown height since the middle Eocene (~38 Ma), classically hypothesized to reflect an evolutionary response to linked climate and vegetation change during the Eocene–Miocene (e.g., Stebbins, 1981; Jacobs et al., 1999; Madden et al., 2010; Strömberg, 2011). Many studies have attempted to test this hypothesis by reconstructing vegetation structure and composition through paleobotanical evidence or indirect proxies (e.g., Croft, 2001; Palazzesi and Barreda, 2012; Strömberg et al., 2013; Dunn et al., 2015). However, most do not explicitly link vegetation

and faunal data to regional and global climate reconstructions to investigate the interplay among global climate change, ocean circulation and local climates and ecologies. Penetrating deep into the southern reaches of Earth's oceans, Patagonia provides an unusual opportunity to do just this. Because South America was effectively separated from other continents from ~50 Ma through the late Miocene to Pliocene (Lawver et al., 2015), its faunas evolved and radiated in relative isolation (Webb, 1978; Simpson, 1980). The resulting, relatively limited impact of immigration is advantageous, because it allows the role of other factors, such as climate change, to be more clearly evaluated.

A classic dichotomy in evolutionary theory distinguishes pressures derived from interactions among co-evolving species (so-called "Red Queen"-type hypotheses[1]; Van Valen, 1973; Bell, 1982) from pressures

---

* Corresponding author. Tel.: +1 208 426 2757; fax: +1 208 426 4061.
E-mail address: mattkohn@boisestate.edu (M.J. Kohn).

---

[1] This hypothesis takes its name from a comment of the Red Queen in Lewis Carroll's "Through the Looking Glass," namely "Now here, you see, it takes all the running you can do, to keep in the same place."

derived from changes to the environment (e.g. climate and tectonics; so-called "Court Jester"-type hypotheses; Barnosky, 2001). The Red Queen has recently been demoted as being of limited use to explain adaptation or extinction, based on both theoretical and empirical considerations (Vermeij and Roopnarine, 2013), and many deep-time studies in both North and South America point to climate as a major driver of evolution, in support of Court Jester hypotheses (Barnosky, 2001; Barnosky et al., 2003; Figueirido et al., 2012; Woodburne et al., 2014). In contrast, other comparative work fails to show any relation between environmental alteration and faunal change (Prothero, 1999, 2004; Alroy et al., 2000); thus the importance of the Court Jester for major evolutionary trends in faunas remains uncertain.

A major shortcoming of virtually all analyses performed so far is the inappropriate spatial scales of the climate data compared to the biotic records, with, for example, regional to continent-wide faunal information assessed against global climate data (e.g., Alroy et al., 2000; Figueirido et al., 2012). Considering the mounting evidence that the nature and timing of faunal and floral changes varied from region to region during the Cenozoic (e.g., Leopold and Denton, 1987; Strömberg, 2005, 2011; Edwards et al., 2010; Finarelli and Badgley, 2010; Woodburne, 2010), region-by-region analysis seems necessary to discern biologically meaningful patterns.

In this study, we sought to improve upon previous work by rigorously evaluating links between abiotic change and biotic responses in southern South America during the Cenozoic (~43 to ~20 Ma), and using the results to assess the strength of the Court Jester. To do so, we combined new stable isotope data with recent and emerging floral and faunal data from a single, confined region in Patagonia, and analyzed these records in the context of global climate change. Specifically, we address the following questions:

1) What was the environment like in central Patagonia in terms of physical climate variables and vegetation structure and composition? How did these change through time?
2) How did global climate change, as represented by the deep marine record, impact local climates? Did abrupt climate shifts, such as the Eocene–Oligocene transition, cause abrupt changes to ecosystems and faunas also in Patagonia? Is there any evidence for local conditions causing feedbacks to global climate?
3) Did climate change impact faunal evolution and if so, what was the timing and rate of that change in relation to climate? In particular, we wish to evaluate whether faunas rapidly (e.g. <1 Ma) adapted tooth morphology to a particular climate and ecological condition, or whether they exhibit significantly delayed response suggesting an evolutionary lag or weak selection (Strömberg, 2006).

2. Background

2.1. Geology

In central Patagonia, a c. 300 meter-thick sequence of fine-grained tuffaceous sediments – the Sarmiento Formation – hosts numerous fossil localities spanning ~43 to ~19 Ma (Kay et al., 1999; G. Ré et al., 2010; G.H. Ré et al., 2010; Dunn et al., 2013). Gran Barranca is the most fossiliferous and famous of these localities and is exposed in southern Chubut Province, Argentina (Fig. 1). Collections from this exposure form the basis for nearly all our interpretations. The Sarmiento Formation overlies middle Eocene intensely pedogenically modified mudstones and tuffaceous sediments of the Koluel–Kaike Formation, and is overlain by Miocene marine sediments of the Chenque Formation (Bellosi, 2010).

Although barren of fossils, paleosols of the Koluel–Kaike Formation provide useful constraints on precipitation (Krause et al., 2010). The age of the Koluel–Kaike Formation is loosely bracketed between ~42 Ma (the oldest overlying age from Gran Barranca; G. Ré et al., 2010) and ~47 Ma (youngest detrital zircon ages from underlying
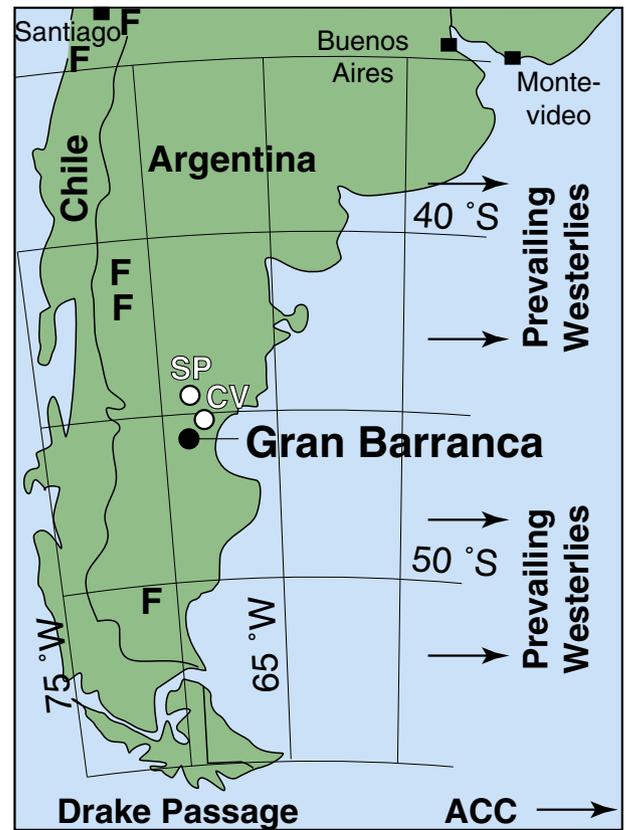

Fig. 1. Location map in South America of Gran Barranca (our primary study area), and secondary locations at Scarritt Pocket (SP) and Cañadon Vaca (CV); F = macrofloral localities (Rio Turbio: 51.5°S, 37–45 Ma; Ñirihuau: 41.3°S, 23–28.5 and 19–23 Ma; Las Aguilas: 33.3°S, 23–26 Ma; Goterones: 33.9°S, ~23 Ma; Los Litres: 33.3°S, 21–23 Ma). Drake Passage and the Antarctic Circumpolar Current (ACC) separate South America physically and oceanographically from Antarctica. The prevailing westerlies blow across (semiarid) Patagonia towards the Southern Oceans.

sediments of the Las Flores Formation; see Supplemental file), and we assume an age of ~45 Ma.

Sarmiento Formation sediments consist dominantly of fine-grained, terrestrial, tuffaceous mudstone, siltstone and fine-grained sandstone, variably reworked via fluvial, eolian and pedogenic processes (Spalletti and Mazzoni, 1979). Zircon trace element patterns are most consistent with an arc source (M. Kohn and J. Crowley, unpubl. data), presumably from the distal Andean arc rather than the more proximal intracontinental backarc. From lowest to highest, the Sarmiento Formation consists of six members: Gran Barranca, Rosado, Lower Puesto Almendra, Vera, Upper Puesto Almendra, and Colhue–Huapi (Fig. 2). The sequence at Gran Barranca spans six successive South American Land Mammal Ages (SALMAs; Madden et al., 2010; Fig. 2); from oldest to youngest these are the Barrancan, Mustersan, Tinguiririran, Deseadan, Colhuehuapian, and Pinturan. The La Cantera level also preserves a faunal assemblage intermediate between Tinguiririran and Deseadan SALMAs. Nearby exposures include (in stratigraphic order) the Itaboraian (Las Flores locality), Riochican (Koluel–Kaike Formation), and Vacan (Cañadon Vaca) SALMAs (e.g., see Woodburne et al., 2014). We generally refer our data to SALMAs in the discussion.

Numerous relatively pristine tuffs occur at Gran Barranca, and basalt flows occur within the Upper Puesto Almendra member. Geochronology of these volcanic rocks combined with magnetostratigraphy defines a detailed chronostratigraphy (G. Ré et al., 2010; G.H. Ré et al., 2010; Dunn et al., 2013) spanning ~42 to ~19 Ma, with the most fossiliferous strata between ~40 and ~20 Ma. Despite its numerous geologic and paleontologic qualities, Gran Barranca does contain major depositional hiatuses (Bellosi, 2010; G. Ré et al., 2010; G.H. Ré et al., 2010), so we
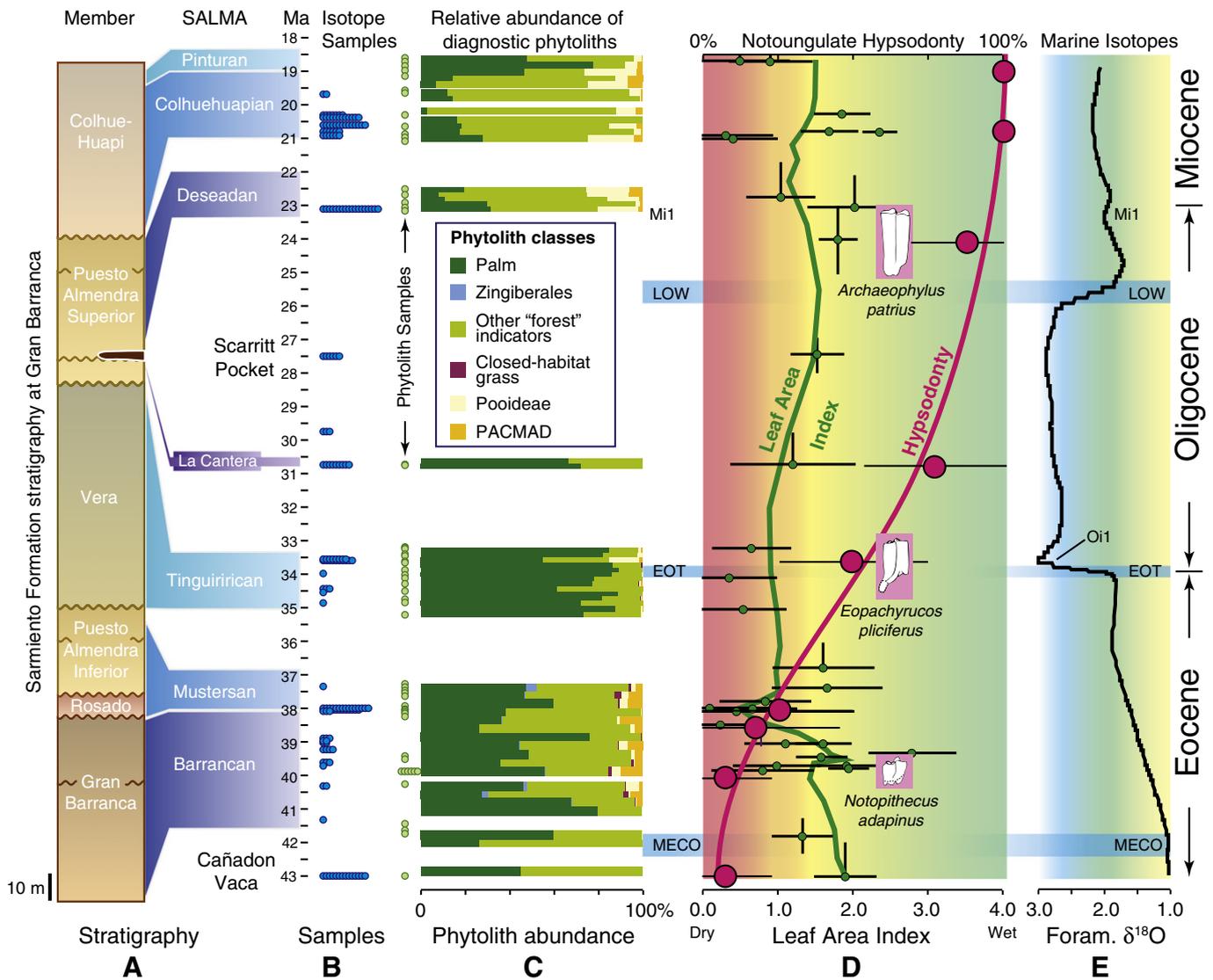
Fig. 2. Published records and sampling levels relevant to this study. (A) Stratigraphy (Dunn et al., 2013). (B) Sampling levels for isotopes. (C) Phytoliths (Strömberg et al., 2013). (D) Reconstructed Leaf Area Index (rLAI) and proportions of hypsodont plus hypselodont notoungulates (Dunn et al., 2015). Age errors (2σ) shown by vertical bars; some are one-sided because chronologic control provides a maximum bound. Where not shown, errors are smaller than symbols; error bars for hypsodonty are bootstrapped 95% confidence intervals. (E) Benthic foraminiferal isotope record (Zachos et al., 2001). MECO = middle Eocene climatic optimum; EOT = Eocene–Oligocene transition; LOW = late Oligocene warming; Mi1 = early Miocene glaciation.

included fossils of different ages from two nearby localities. Fossils from basal Sarmiento Formation at Cañadon Vaca (Fig. 1) define the Vacan SALMA (Cifelli, 1985; ~43 Ma; Fig. 2), and fossils from Scarritt Pocket (Fig. 1) are from the early Deseadan (27.2 Ma; Vucetich et al., 2014; Supplemental file; Fig. 2). These localities are sufficiently close to Gran Barranca that we do not expect significant differences in climate; for example, modern climatic conditions are indistinguishable.

2.2. Floras

Although plant macrofossils are spectacularly well preserved prior to the middle Eocene in southern South America (e.g. see Wilf et al., 2013), occurrences are temporally sporadic from the late Eocene through Miocene (Hinojosa and Villagrán, 2005). Instead phytoliths (microscopic silica particles formed inside living plants) provide a more continuous record of floras for the post-middle Eocene (Strömberg et al., 2013; Fig. 2). These microfossils show that grasses were remarkably sparse between 43 and 18.5 Ma, especially during the latest Eocene to middle Oligocene, and instead palms, conifers, and "forest" indicators (collectively "dicots," ferns, conifers, and gingers) dominate. Grass abundances were slightly higher

in the mid/late Eocene (up to ~15% of phytolith assemblages) and increased in the early Miocene (up to ~25% of phytolith assemblages; Strömberg et al., 2013). These data conclusively rule out the occurrence of grasslands through the sequence analyzed. However, although phytolith and sparse pollen data were originally interpreted as indicating relatively closed, forested habitats (Palazzesi and Barreda, 2012; Strömberg et al., 2013), new research on phytolith micromorphology (Dunn et al., 2015) implies that Patagonian plant communities experienced high light levels characteristic of relatively open habitats. In the absence of abundant grasses, phytolith and pollen types alone do not necessarily indicate habitat openness, and habitats could have ranged from closed to relatively open.

2.3. Faunas

The Sarmiento Formation preserves a rich record of faunas and faunal evolution. Of special relevance to this study, between ~40 and ~20 Ma increases are observed in both mean tooth crown height (hypsodonty or the ratio of tooth crown height to anterior–posterior length, here determined on relatively unworn M1 molars) within clades

and the proportion of taxa among notoungulates with high-crowned (hypsodont) and ever-growing (hypselodont) teeth (Fig. 2; Strömberg et al., 2013; Dunn et al., 2015). In general, Patagonian faunas show increases in hypsodonty earlier than at other sites in South America (Strömberg et al., 2013), so we view these changes as occurring in situ rather than simply reflecting immigration of taxa that evolved elsewhere. Increases in hypsodonty (and many other characteristics such as cursoriality) parallel but significantly precede (by 15–20 Ma) similar changes observed in northern hemisphere ungulates (Webb, 1977, 1978; Jacobs et al., 1999).

Hypsodonty was originally viewed as an adaptation to grazing in grassland ecosystems (e.g., Kovalevsky, 1874; Scott, 1937; Stebbins, 1981; see review of Damuth and Janis, 2011). Most researchers today, however, identify the main selective agent for hypsodonty as the incidental ingestion of abrasive soil or grit resulting from feeding close to the ground in generally open habitats, not necessarily grasslands (Williams and Kay, 2001; Sanson et al., 2007; Damuth and Janis, 2011; Kaiser et al., 2013; Madden, 2014). Thus, hypsodonty could certainly evolve in the context of grasslands (e.g., Strömberg, 2006; Strömberg et al., 2007), but could alternatively evolve in any dusty or gritty environment. Phytolith analysis at Gran Barranca and Cañadon Vaca supports this view by demonstrating that evolution of hypsodonty among notoungulates in Patagonia occurred in vegetation types lacking major grass biomass (Fig. 2; Strömberg et al., 2013).

2.4. Climate

The long interval represented by strata in central Patagonia spans significant climate change (e.g. Zachos et al., 2001), notably gradual cooling from the mid-Eocene Climatic Optimum (MECO; ~42 Ma) to the late Eocene, abrupt cooling across the Eocene–Oligocene transition (EOT; 33.5–34 Ma) and possible late Oligocene warming (LOW: 25–26 Ma). The EOT is widely viewed as a global response to the tectonic isolation of Antarctica and development of the Antarctic Circumpolar Current (Kennett, 1977). The origins and global significance of LOW are debatable as studies proximal to Antarctica show nearly constant bottom water temperatures and evidence for full glaciation (Pekar et al., 2006). LOW may simply reflect a decrease in the export of cold Antarctic bottom waters to the Atlantic and Pacific, allowing their deep waters to warm, rather than a global increase in temperature (Pekar et al., 2006).

The effects of these events on Patagonian climate are not well known. Sparse Patagonian megafloras provide constraints for the middle Eocene to early Miocene of southern South America (Hinojosa and Villagrán, 2005), but few have good age control, obscuring an exact climatic pattern for the period of interest. Leaf physiognomy-based estimates suggest a relatively stable MAT of 17 ± 3 °C from the late middle Eocene (37–45 Ma) to earliest Miocene (~21 Ma) with substantially higher temperatures (23–25 °C) for the middle Miocene (10–19 Ma; adjusted values from Hinojosa, 2005, using MAT correction in Hinojosa et al., 2011, and age correction in Dunn et al., 2015). The same sparse record suggests that MAP dropped during the middle Cenozoic, from >2000 mm in the middle Eocene to ~1000 mm by the latest Oligocene, but the exact timing of this decrease is unclear and errors are large (c. +65%/−40%; Hinojosa, 2005; Hinojosa and Villagrán, 2005; Hinojosa et al., 2006). Pollen data are consistent with relatively warm, humid climates until the late Oligocene (Barreda and Palazzesi, 2007; Quattrocchio et al., 2013). Paleosol character for the late Eocene Koluel–Kaike Formation near Gran Barranca similarly points to aridification, but much earlier during the middle Eocene, resulting in a MAP of 600–700 mm/yr by ~44 Ma (Krause et al., 2010). Estimates of MAP at Gran Barranca have been based on paleosol character in the context of assumed floras, and range between 300 and 1100 mm/yr (Bellosi and González, 2010).

2.5. Previous stable isotope work

Previous stable isotope work for this time interval in central Patagonia primarily consists of oxygen isotopes in fossil teeth (Kohn et al., 2004, 2010). These data suggest only small changes in $\delta^{18}O$ through the section, interpreted to reflect only small changes in temperature (Kohn et al., 2004, 2010), consistent with paleobotanical data (Strömberg et al., 2013; Dunn et al., 2015; see discussion below). The present study significantly expands the isotope dataset, lending confidence to $\delta^{18}O$ trends. More importantly, we have also measured $\delta^{13}C$ values of tooth enamel, $\delta^{18}O$ values of coexisting fossil bone, and $\delta^{18}O$ and $\delta^{13}C$ of pedogenic carbonate, from which MAP, p_{CO2}, and temperature changes can be estimated (Cerling, 1991, 1999; Zanazzi et al., 2007; Kohn, 2010). These new observations in turn permit intercomparisons among faunal evolution, local climate, local environment, and global climate.

3. Methods

3.1. Sampling

Previously analyzed fossil teeth (Kohn et al., 2004, 2010) were precisely located relative to distinctive tuffs. The teeth are all identifiable to family, commonly to genus, and occasionally to species. We collected new fossil tooth enamel and bone specimens at Cañadon
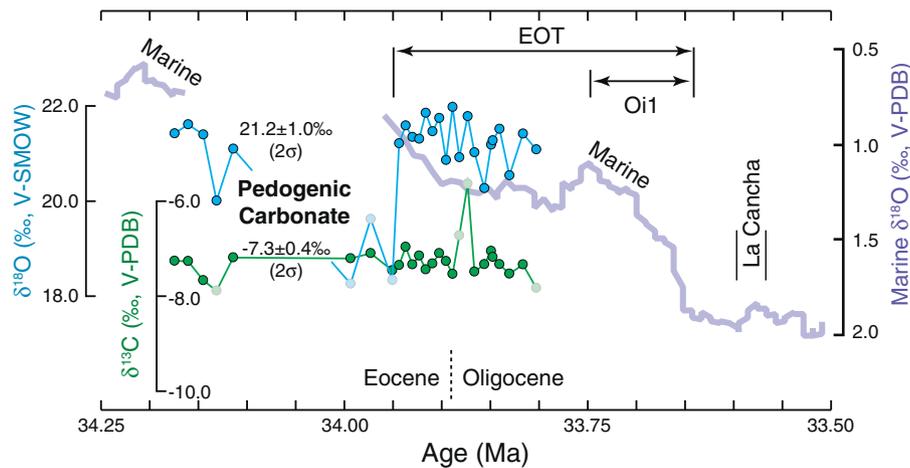

Fig. 3. Stable isotope data from pedogenic carbonate within the Vera member, immediately prior to the biggest cooling step of the EOT (Oi1; Miller et al., 1991), showing nearly constant compositions. Light-colored symbols are compositional outliers. Marine curve is from benthic foraminiferal analyses of Coxall et al. (2005). A hiatus in that record occurs between 34.15 and 33.95 Ma. La Cancha is precisely dated (Dunn et al., 2013), particularly fossiliferous horizon in the Gran Barranca section with early Tinguiririran faunas.

Vaca and Gran Barranca mostly from float, prospecting along ridge axes rather than ridge bases or flat areas to minimize downward drift and time-averaging of fossils. A similar approach (Zanazzi et al., 2009) proved successful in delineating abrupt isotope shifts elsewhere (Zanazzi et al., 2007; Zanazzi and Kohn, 2008). We also collected pedogenic carbonate nodules through a subsection of the lower Vera member near the Eocene–Oligocene boundary. All specimens were located to the nearest 0.1–0.25 m using a Jacobs staff relative to distinctive tuffs, which were located within the overall chronostratigraphic framework of Dunn et al. (2013). Note that because of slight variations in thickness along different transects, our meter levels do not always line up precisely with Dunn et al.'s, but key chronologic horizons are identical. Ultimately we average many of our data into time slices, so these minor differences are unimportant.

Tooth enamel fragments were also collected from Cañadon Vaca from a fossiliferous tuff, geographically isolated from the stratigraphically coherent section. Attempts to separate and date zircons from the tuff were unsuccessful, so we simply assign an average age of ~43 Ma to all specimens; this age is intermediate between the VRS tuff at Gran Barranca (41.7 Ma; G. Ré et al., 2010), which stratigraphically overlies the Vacan, and the assumed age of the Koluel–Kaike Formation (~45 Ma). Teeth from Scarritt Pocket were obtained from past collections housed at the Museo de la Plata. Fossils and tuff were collected from a single horizon, so we assign a single age of 27.2 ± 0.5 Ma (Vucetich et al., 2014).

Few of the new enamel fragments could be identified to genus or species, but microstructural characteristics combined with previous studies of faunas help delineate likely families. For example, thick enamel (≥ 2 mm thickness) with tiny transverse ridges on occlusal surfaces is characteristic of astrapotheres, whereas the occurrence of perikymata (transverse ridges on outer tooth surfaces) is restricted to toxodontids, and enamel from large brachydont to mesodont teeth is probably derived from leontiniids or isotemnids (two extremely common families). These distinctions facilitate comparison of isotope compositions among different families.

For each tooth enamel fragment, we subsampled a thin sliver along its growth axis, favoring longer fragments where possible, and powdered the entire sliver for isotope compositions. This approach averages isotope zoning, but previous studies have explored zoning for many levels (Kohn et al., 2004, 2010), and variation among numerous different specimens provides an alternate measure of isotope variability for a particular time slice. For comparison equivalency, we average isotope compositions of each serially-sampled tooth from previous studies to a single composition. Isotope composition of bones are commonly quite scattered (e.g. Zanazzi et al., 2007, 2009), so for each level we powdered small fragments of individual bones, pretreated separately, then mixed equal amounts (1 mg) into a composite for analysis. Strictly speaking, bone compositions must post-date enamel compositions slightly because of the time needed to diagenetically alter the bone (c. a few tens of ka; see Kohn and Law, 2006). Such a small time difference is not resolvable in our sampling or dataset. We attempted to sample 5 bone specimens per level, but several levels were bone-poor, so composites ranged from 1 to 5 individual bone fragments, on average 4. For teeth from Scarritt Pocket, we cut longitudinal slivers on site at Museo de la Plata using a small rock saw, mounted slivers on glass slides using acetone-soluble cement, and subsampled every ~1–2 mm along the length of the sliver using a slow-speed saw. Individual subsamples were then powdered for analysis.

Pedogenic carbonate nodules were prepared and analyzed for stable carbon and oxygen isotopes at the Boise State Stable Isotope Laboratory. Nodules were collected with an ~0.2 m spacing from ~33 to ~44 m above the base of the Vera (34.2 to 33.8 Ma), with a gap between ~35 and ~38 m (34.1 to 34.0 Ma; Fig. 3). These levels underlie the precisely dated, fossiliferous La Cancha level (c. 50 m above the member base; 33.58 Ma; Dunn et al., 2013), and fall within the earliest stage of the EOT immediately prior to the main Oi1 phase (Fig. 3). Carbonate

nodules were not found elsewhere along our transect and are randomly distributed, which we interpret to reflect continuous aggradation of superposed Bk horizons (Bk refers to the level of carbonate accumulation in a soil; Soil Survey Staff, 2010). Texturally analogous nodules from the Vera are illustrated in (Bellosi and González, 2010; their Fig. 20.2-9; see Supplemental file).

3.2. Isotope analysis

Fossil tooth, bone, and reference NIST120c powders were identically pretreated using the method of Koch et al. (1997) and analyzed for $\delta^{13}C$ and $\delta^{18}O$ values of structural carbonate (Table 1) using an automated extraction system (Gasbench II) attached to a ThermoFisher Delta V-Plus mass spectrometer housed in the Stable Isotope Laboratory, Department of Geosciences, Boise State University. Pedogenic carbonate nodules consist solely of micritic calcite (no sparry calcite was found), so a small portion was powdered and analyzed using the same analytical system. Raw data were standardized against NIST18 and NIST19 carbonates, whose analytical reproducibilities for both C- and O-isotopes were ± 0.2–0.3‰ ($\pm 2\sigma$). Biogenic phosphate $\delta^{18}O$ values exhibit small but systematic session-to-session variations in absolute values. Consequently, we made further small corrections based on concurrent analysis of NIST120c (a phosphorite with broadly similar bioapatite chemistry as fossil teeth and bones), assuming a composition of 28.50‰ (V-SMOW) based on an ~10 year average of analyses collected in our laboratory. Average values for NIST120c $\delta^{18}O$ range from 28.2 to 28.8‰ (V-SMOW). Carbon isotope values require no additional correction and for NIST120c average −6.55‰ (V-PDB). Reproducibility on NIST120c was approximately ± 0.25‰ for $\delta^{13}C$ and ± 0.6‰ for $\delta^{18}O$ (2σ).

3.3. Temperature calculations from fossil bones and teeth

The fractionation of oxygen isotopes between fossil bone and enamel can potentially elucidate changes in air (soil) temperature (Zanazzi et al., 2007) because bone is diagenetically altered at ambient soil temperatures (Kohn and Law, 2006) whereas enamel retains its original composition imparted at mammal body temperature (i.e. 37 °C). The approach of Zanazzi et al. (2007) and modern calibrations for Bovinae and Equidae (Kohn and Dettman, 2007; Kohn and Fremd, 2007) yield the following equation:

$$T(°C) = \frac{18030}{1000 \ln\left(\frac{1 + \left(\delta^{18}O_{bone} - 2.2\right)/1000}{1 + \left(1.15 \cdot \delta^{18}O_{enamel} - 36.3\right)/1000}\right) + 32.42} - 273.15 \qquad (1)$$

where $\delta^{18}O$ of bone and enamel is expressed on the V-SMOW scale.

3.4. MAP calculations

Carbon isotope values of C_3 plants and their consumers track the $\delta^{13}C$ of atmospheric CO_2, but also correlate negatively with MAP (e.g., Stewart et al., 1995). These dependencies were calibrated using modern data to permit calculation of MAP (Kohn, 2010):

$$MAP = 10^{\left[\frac{\Delta^{13}C - 2.01 + 0.000198 \cdot elev - 0.0129 \cdot Abs(lat)}{5.88}\right]} - 300 \quad (2)$$

where elev = elevation in meters, lat = latitude in degrees, and

$$\Delta^{13}C = \frac{\delta^{13}C_{atm} - \delta^{13}C_{leaf}}{1 + \delta^{13}C_{leaf}/1000} \qquad (3)$$

where $\delta^{13}C_{atm}$ and $\delta^{13}C_{leaf}$ are the carbon isotope compositions of atmospheric CO_2 and vegetation, respectively, as determined from proxies. The benthic foraminiferal record provides a proxy for $\delta^{13}C_{atm}$

Table 1
Summary of mean isotope compositions, $\delta^{13}C$ of atmospheric CO_2, and calculated MAP.

Time slice	$\delta^{18}O_e \pm 2$ s.e.	$\delta^{18}O_b \pm 2$ s.e.	$\delta^{13}C_e \pm 2$ s.e.	$\delta^{13}C_b \pm 2$ s.e.	$\delta^{13}C_a$	MAP $\pm 2\sigma$	T (°C) ± 2 s.e.
Vacan	23.25 ± 0.67	22.06 ± 0.39	-10.65 ± 0.42	-8.44 ± 0.29	-5.85	390 ± 120	19.1 ± 4.1
Barrancan	22.39 ± 0.88	22.52 ± 0.33	-11.36 ± 0.48	-9.43 ± 0.22	-5.97	590 ± 180	12.4 ± 4.9
Barrancan − anom.	21.85 ± 1.24	n.a.	-10.81 ± 0.45	n.a.	-5.97	420 ± 130	
Mustersan	23.07 ± 0.77	22.87 ± 0.49	-11.15 ± 0.56	-8.53 ± 0.32	-6.20	450 ± 170	14.4 ± 4.7
Tinguirirican (ave)	23.32 ± 0.54	n.a.	-10.54 ± 0.55	n.a.	-5.75	400 ± 160	
Tinguirirican (early)	23.45 ± 0.57	22.61 ± 0.64	-10.74 ± 1.30	-9.74 ± 0.43	n.a.	n.a.	17.7 ± 4.3
Tinguirirican (late)	23.28 ± 0.69	n.a.	-10.43 ± 0.51	n.a.	n.a.	n.a.	
La Cantera	23.77 ± 0.65	n.a.	-11.27 ± 0.46	n.a.	-6.07	530 ± 160	
Deseadan (early)	23.02 ± 0.78	n.a.	-10.22 ± 0.77	n.a.	-6.27	200 ± 160	
Deseadan (late)	21.97 ± 0.27	n.a.	-11.55 ± 0.44	n.a.	-5.88	700 ± 180	
Colhuehuapian	23.01 ± 0.28	22.71 ± 0.34	-11.98 ± 0.36	-9.91 ± 0.22	-6.09	800 ± 160	14.8 ± 2.1

Note: Isotope compositions are in permil relative to V-SMOW ($\delta^{18}O$) and V-PDB ($\delta^{13}C$). MAP = mean annual precipitation in mm/yr (rounded to nearest 10 mm). Subscripts: e = enamel, b = bone, a = atmospheric CO_2. Barrancan − anom. shows the means after removing anomalously low $\delta^{13}C$ data from a specific horizon. For Tinguirirican data, ave = all data, early = prior to the EOT, late = after the EOT. Temperature calculations propagate errors in isotope compositions only.

(Tipple et al., 2010). Although we have no direct measure of plant compositions, tooth enamel in modern perissodactyls (horses, rhinos, and tapirs) exhibits a constant, ~14‰ offset relative to diet (Cerling and Harris, 1999). Perissodactyls are hindgut fermenters, retaining the plesiomorphic digestive physiology. Recent fossil protein sequence analysis linking South American (meridi)ungulates most closely to crown Perissodactyla (Buckley, 2015; Welker et al., 2015) and the strong similarities in cranio-dental morphology between perissodactyls and notoungulates (Fletcher et al., 2010; Cassini et al., 2012), suggest that notoungulates were also hindgut fermenters and justifies use of a similar offset to estimate plant $\delta^{13}C$ values and hence MAP (Kohn et al., 2010). That is, $\delta^{13}C_{leaf} = \delta^{13}C_{tooth\ enamel} - 14‰$. Note that CAM plants neither form a large biomass component in most ecosystems nor are consumed in quantity by most herbivores, and that C_4 plants were absent or at least very rare until long after the time period of interest (Cerling et al., 1997; Edwards et al., 2010; Strömberg, 2011).

Mean annual precipitation was calculated from carbon isotope compositions of tooth enamel by first subtracting 14‰ to determine $\delta^{13}C_{leaf}$, then applying Eqs. (2) and (3), basing $\delta^{13}C_{atm}$ on Tipple et al. (2010). In principle, MAP above 1700 mm/yr may be difficult to quantify because very dense forests have anomalously low $\delta^{13}C$ values (-32 to $-37‰$ in modern ecosystems; see Kohn, 2010). Inferred $\delta^{13}C_{leaf}$ values in this study are well above any likely closed forest values, however, so no additional correction is needed. Random uncertainties are propagated based on compositional scatter of the isotope data (standard errors). Systematic errors in the MAP calibration are approximately $\pm 50\%$ (2σ) of the absolute value (Kohn and McKay, 2012). We made no correction of $\delta^{13}C$ for p_{CO2} because corrections (Schubert and Jahren, 2012) applied to published tooth enamel data worldwide imply negative MAP for the Oligocene, implausibly low MAP (≤350 mm/yr) for demonstrably wet periods of the Paleocene, Eocene and Miocene, and implausibly high MAP (≥2000 mm/yr) for the relatively dry Pleistocene (Kohn, 2014). Similarly, many tree ring isotope studies covering the last century do not independently resolve a p_{CO2} effect on isotope discrimination (e.g., Saurer et al., 2004). Other estimates of MAP in South America were taken from studies of leaf physiognomy for sites 300–700 km NW of the study area (Fig. 1; Hinojosa, 2005; Hinojosa and Villagrán, 2005; Hinojosa et al., 2011) and from paleosols of the Koluel–Kaike Formation (Krause et al., 2010) and the Sarmiento Formation at Gran Barranca (Bellosi and González, 2010). The latter estimates, however, may be biased by local sediment accumulation rates (see further discussion below).

3.5. p_{CO2} calculations

The $\delta^{13}C$ of pedogenic carbonate can be used to estimate p_{CO2} provided the following compositional and concentration parameters are constrained (Cerling, 1991, 1999): the concentration of soil CO_2 [S(z)] and values for $\delta^{13}C_s$, $\delta^{13}C_\Phi$ and $\delta^{13}C_a$, where subscripts s, Φ, and a refer to soil CO_2, respired CO_2 (commonly taken as soil organic carbon $\delta^{13}C$), and air CO_2:

$$p_{CO_2} = S(z)\left[\frac{\delta^{13}C_s - 1.0044 \cdot \delta^{13}C_\Phi - 4.4}{\delta^{13}C_a - \delta^{13}C_s}\right]. \quad (4)$$

We estimated $\delta^{13}C_s$ (soil CO_2) from measured mean pedogenic calcite as corrected for formation temperature according to experimental calibrations (Romanek et al., 1992):

$$1000\left[\left(\frac{\delta^{13}C_{CaCO_3} + 1000}{\delta^{13}C_{CO_2} + 1000}\right) - 1\right] = 11.98 - 0.12 \cdot T(°C). \quad (5)$$

Because organic carbon contents of these sediments are extremely low, our preferred value for $\delta^{13}C_\Phi$ is based on mean $\delta^{13}C$ values of tooth enamel carbonate ($-10.5 \pm 0.5‰$; Kohn et al., 2010, this study), corrected downward by 14‰ for leaf-enamel fractionation (Cerling and Harris, 1999) and corrected upward by $2 \pm 1‰$ for the difference between bulk leaf vs. soil organic matter in modern soils (Bowling et al., 2008). The value for $\delta^{13}C_a$ is again based on benthic foraminiferal records (Tipple et al., 2010). For S(z), recent work suggests a typical value during pedogenic carbonate precipitation of 2500 ± 1000 ppm (Breecker et al., 2010). A regression of S(z) vs. MAP (Cotton and Sheldon, 2012) implies a similar S(z) of ~2300 ppm, using MAP values determined from isotope data (see below) and paleosol character in the Vera Member (Bellosi and González, 2010; 300–650 mm/yr).

4. Results

Isotope compositions of pedogenic carbonate nodules are remarkably homogeneous through the c. 400 ka section analyzed (Fig. 3). Omitting a few outliers at low $\delta^{18}O$ and high $\delta^{13}C$, which may reflect nodules that formed closer to paleosurfaces, average values are $\delta^{13}C = -7.3 \pm 0.4‰$ (V-PDB; 2σ) and $\delta^{18}O = 21.2 \pm 1.0‰$ (V-SMOW; 2σ). These are some of the first isotope data from definitive pedogenic carbonates collected proximal to the EOT, and $\delta^{13}C$ values are well within the range reported globally for Eocene and Oligocene paleosols (Ekart et al., 1999; Sheldon and Tabor, 2009; Sheldon et al., 2012; Srivastava et al., 2013). In combination with published tooth enamel $\delta^{18}O$ and $\delta^{13}C$ values, p_{CO2} and paleotemperature may be estimated.

Compositions for enamel and bone scatter by ~$\pm2‰$ for both carbon and oxygen for each time slice (Fig. 4A–B). Such scatter is expected mainly because of intra-tooth zoning that encodes seasonal isotope
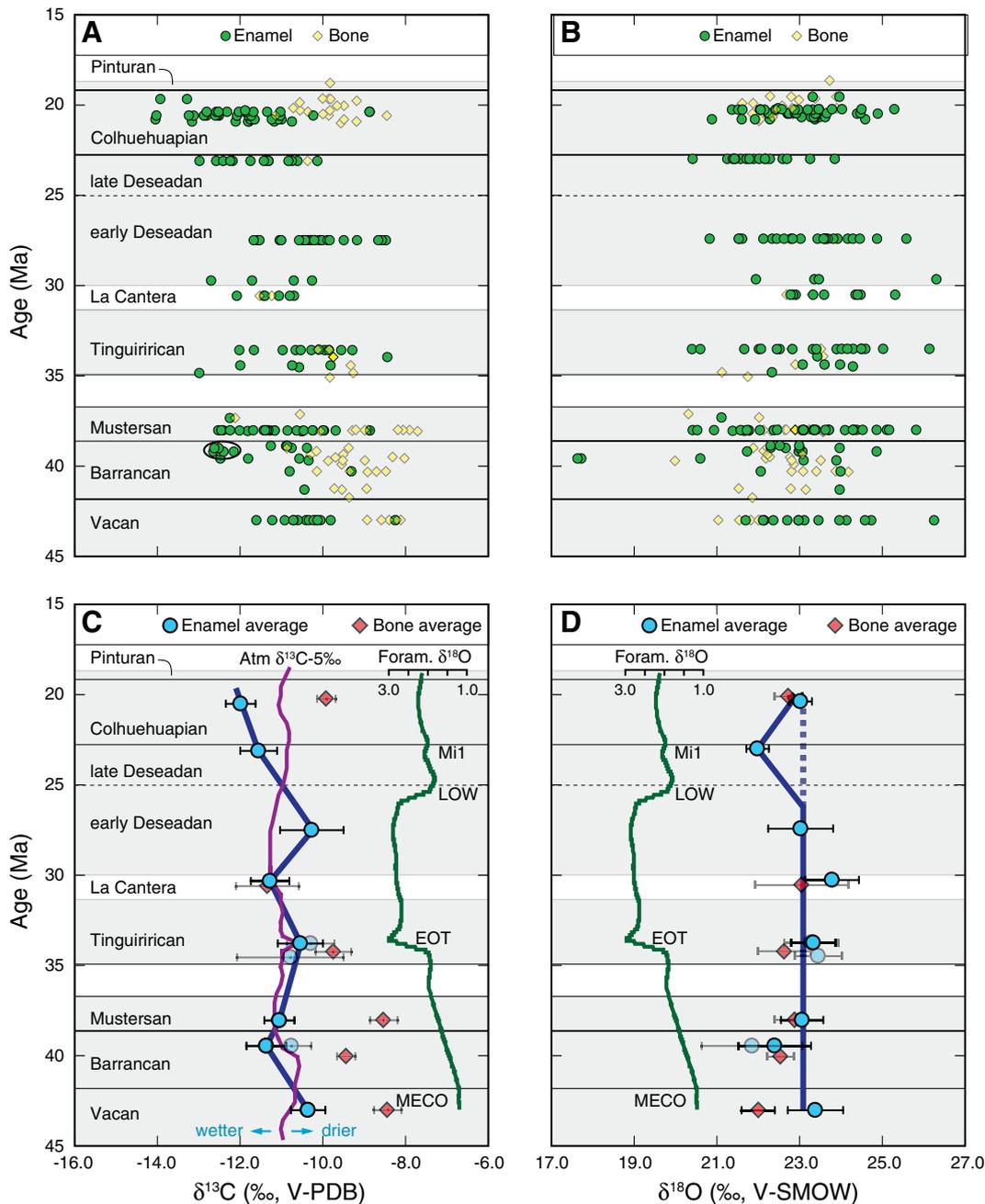
Fig. 4. Stable isotope data from fossil tooth enamel and bone. (A–B) Raw data for individual tooth enamel fragments and bone composites for carbon isotopes (A) and oxygen isotopes (B), illustrating broadly comparable data ranges through time. Small ellipse in A emphasizes cluster of anomalously low $\delta^{13}C$ values during a specific short interval (39.2 to 39.0 Ma). (C–D) Time-slice averages with reference global atmospheric (Tipple et al., 2010) and deep marine curves (Zachos et al., 2001). Light blue symbols in Barrancan show the effect of removing cluster of anomalous $\delta^{13}C$ values from mean; light blue symbols in Tinguiririran distinguish the compositions immediately pre- and post-EOT. Error bars are ±2 s.e. Relative to atmospheric $\delta^{13}C$ values minus 5‰, tooth enamel $\delta^{13}C$ values are generally comparable or slightly higher until 27.2 Ma then significantly lower. Enamel $\delta^{18}O$ values are indistinguishable through time except at ~23 Ma. Bone $\delta^{18}O$ values are not significantly different from enamel except for the Vacan.

variations, but also because of year-to-year variations in climate. Scatter in $\delta^{18}O$ shows no significant differences at 95% confidence (F-tests, applying Bonferroni correction) except for $\delta^{18}O$ of Barrancan vs. late Deseadan and Colhuehuapian times (Supplemental file). However, omitting two anomalous compositions from the Barrancan data eliminates these differences, and bone compositional scatter is indistinguishable for the Barrancan and Colhuehuapian. Overall we infer comparable scatter at different times. Differences in variance among identifiable taxa for specific time slices are also not significant (Supplemental file).

We found no significant differences in mean $\delta^{13}C$ or $\delta^{18}O$ values among different sympatric families (data in Supplemental file), so discuss isotope compositions as averaged across taxa. Average enamel $\delta^{13}C$ generally tracks $\delta^{13}C$ of atmospheric CO_2 for the earlier half of the record (Fig. 4C), but is slightly higher in the early Deseadan and deviates to lower $\delta^{13}C$ values for the later Deseadan and Colhuehuapian. Average bone $\delta^{13}C$ values scatter widely. Average enamel $\delta^{18}O$ values show no significant differences among levels except for the later Deseadan, which is significantly lower (Fig. 4D). Excepting Vacan specimens, bone $\delta^{18}O$ values do not differ significantly from enamel values.

5. Discussion

5.1. Oxygen isotopes and Patagonian paleoclimate

Our expanded dataset corroborates previous studies (Kohn et al., 2004, 2010) that showed no significant change to $\delta^{18}O$ values through the section, except during Deseadan time. Note that Kohn et al. (2010) assumed an age for the Deseadan fossils at Gran Barranca of ~27 Ma, but the fossils occur along a disconformity whose age is bracketed between 26.3 ± 0.3 and ≤23.1 Ma (Ré et al., 2010a; Dunn et al., 2013). Regardless, these fossils postdate Deseadan faunas at Scarritt Pocket (27.2 Ma; Vucetich et al., 2014). The climatic implications of constant $\delta^{18}O$ values must be considered in the context of changes to global ocean $\delta^{18}O$ attending changes in ice volume. Specifically, growth of the Antarctic ice sheet during the EOT should have raised ocean and precipitation $\delta^{18}O$ values by ~1‰ (Coxall et al., 2005). One possible reason this increase is not observed is that decreasing temperature normally decreases precipitation $\delta^{18}O$ values, with a coefficient of ~0.35‰/°C at mid- to high latitudes (see Kohn et al., 2002). Correlations between biogenic phosphate and local water $\delta^{18}O$ (e.g. Kohn, 1996; Kohn and Cerling, 2002) imply an ~0.3‰ decrease in enamel $\delta^{18}O$ per degree of cooling. Thus, constant $\delta^{18}O$ values across the EOT in the context of a 1‰ rise in the global meteoric system could indicate a temperature decrease of c. 3–4 °C (1‰ ÷ 0.3‰/°C; Kohn et al., 2010). Alternatively, small changes to moisture sources at constant temperature could have offset the global increase in water $\delta^{18}O$. For example, changes in the position and intensity of the westerlies have been documented during the Quaternary, affecting plant communities and hydrology (e.g., Moreno et al., 2012). Similar changes might have influenced isotope compositions to offset the global shift independent of temperature. Constant $\delta^{18}O$ values subsequent to the EOT are consistent with quasi-constant temperatures and ice volume through the Oligocene and (arguably) the early Miocene, supporting previous suggestions that late Oligocene warming was not manifest at high southern latitudes (Pekar et al., 2006). Even if late Oligocene warming was a global phenomenon, high ice volume in Antarctica (i.e. quasi-constant global ocean compositions; Pekar et al., 2006) may indicate that temperature did not change significantly in central Patagonia. A constant temperature is consistent with indistinguishable MAT estimates for late Eocene through early Miocene floras in southern South America (Hinojosa and Villagrán, 2005; Hinojosa et al., 2006, 2011; see discussion below).

The ~1.1‰ dip in $\delta^{18}O$ values for late Deseadan fossils at Gran Barranca might reflect deep glaciation associated with Mi1 at 23 Ma (Miller et al., 1991). Because the disconformity from which the fossils derive spans at least 3 Ma, we cannot definitively pin the isotopes to this event. But possibly abrupt cooling catalyzed erosion of underlying sediments and accumulation of teeth. If so, the isotope shift would be consistent with brief cooling of at least 4 °C (1.1‰ ÷ 0.3‰/°C).

Application of Eq. (1) (above) to bone and enamel compositions through the sequence (Fig. 4) implies relatively constant alteration temperatures of 16 ± 3 (2 s.e.) °C. Unfortunately we lack bone from after the EOT to independently test interpretations of temperature changes derived from oxygen isotope trends alone. Calculated temperatures are lower than body temperature because, although isotope compositions are comparable for bone and enamel, body water $\delta^{18}O$ for large, water-dependent herbivores is typically at least 5‰ higher than local water (e.g. Kohn and Cerling, 2002). That is, enamel and bone $\delta^{18}O$ values may be similar, but the water $\delta^{18}O$ values with which the bioapatite equilibrated differed considerably. We assume that bone does not preserve original biogenic compositions because its $\delta^{13}C$ values are substantially different from enamel in many levels. The calculated alteration temperature is higher than modern day MAT (11.0 °C for Sarmiento, Argentina), and overlaps temperatures estimated from marine and floral data of the mid-Cenozoic. Models of ocean circulation anchored to measurements of temperature from bivalve shells spanning 34 to 45 Ma imply essentially constant MAT = 15–17 °C for coastal South America at the latitude of Gran Barranca (Douglas et al., 2014). Insofar as temperature in Patagonia is strongly buffered by proximity to the ocean, Douglas et al.'s observations and our new isotope data imply that temperatures in the region decreased relatively little between the Eocene and early Miocene. Floral analysis similarly implies statistically indistinguishable MAT values of 17 ± 3 °C from the Eocene through early Miocene (Hinojosa and Villagrán, 2005; Hinojosa et al., 2006), although later calculations using leaf physiognomy methods calibrated to South American floras produce MAT values that are ~1.5 °C lower (Hinojosa et al., 2011). A value for MAT of 14–18 °C fits observations for all data except the late Deseadan.

Variation in $\delta^{18}O$ is commonly taken to reflect changes in local water $\delta^{18}O$, which in turn responds to temperature. For example, $\delta^{18}O$ zoning in teeth closely tracks seasonal meteoric water composition, which correlates with seasonal temperature (e.g., Fricke and O'Neil, 1996; Kohn, 1996). In general, our sampling protocol did not resolve sufficient fine-scale detail to warrant close comparisons among levels. However, the ±2‰ range divided by the temperature coefficient for seasonal isotope variations in large herbivores at mid-latitudes (0.3‰/°C; Zanazzi et al., 2007) implies a minimum estimate of the mean annual range of temperature (MART) of ~13 °C, identical to estimates of MART derived from Eocene through early Miocene floras of southern South America (13–14 °C; Hinojosa and Villagrán, 2005). In combination with a MAT of 16 °C, this range implies a warm-month mean temperature (WMMT) of 23 °C. The range of variation does not appear to differ significantly among levels, implying similar MART through the sequence.

The $\delta^{18}O$ of pedogenic calcite can also be used to infer temperature, if the $\delta^{18}O$ of soil water is known independently. This temperature is expected to reflect WMMT because pedogenic carbonate forms preferentially during the dry (usually warmest) season (Breecker et al., 2009). Tooth enamel $\delta^{18}O$ correlates closely with local water $\delta^{18}O$ (e.g. see review of Kohn and Cerling, 2002), so we used $\delta^{18}O$ values for tooth enamel from the Vera Member (Kohn et al., 2010; this study) and global correlations for water-dependent ungulates (Kohn and Cerling, 2002; Kohn and Dettman, 2007; Kohn and Fremd, 2007) to derive local water $\delta^{18}O$. Because we infer a plesiomorphic hindgut digestive physiology for meridiungulates (see above) we reasonably assume that they were water dependent like all perissodactyls today (McNab, 2002). These data imply a local water composition of $\sim -8.5 \pm 1.0$‰ (V-SMOW), with the largest uncertainty resulting from scatter in modern correlations. Together with a mean pedogenic calcite value of 21.3 ± 0.2‰ (V-SMOW, 2 s.e.), the experimental calibration of Kim and O'Neil (1997) implies a precipitation temperature of 18 ± 6 °C. This temperature overlaps with but is slightly lower than WMMT independently estimated above from MAT, MART, and sea-surface temperature (~23 °C). Increasing assumed soil water $\delta^{18}O$ by 1‰ (e.g., reflecting modern calibration errors or soil water evaporation) would increase calculated WMMT by 5 °C and reconcile all temperature calculations.

5.2. Pedogenic carbonate and p_{CO2}

For calculating p_{CO2}, we estimated $\delta^{13}C_s$ (−16.5‰) from pedogenic carbonate $\delta^{13}C$ (−7.3 ± 0.1‰) assuming carbonate formed at a WMMT temperature of 23 °C. Other parameters include $\delta^{13}C_a = -6.0$‰ (Tipple et al., 2010) and $\delta^{13}C_{\phi} = -22.5 \pm 1$‰ based on mean $\delta^{13}C$ values of tooth enamel carbonate (−10.5 ± 0.5‰; Kohn et al., 2010; this study) and offsets between bulk leaves and soil organic matter (Bowling et al., 2008). Taken together, these values imply $p_{CO2} = 430 \pm 250$ ppmv, indistinguishable from estimates from mid-Oligocene paleosols in India (433 and 633 ppmv, uncertainties not reported; Srivastava et al., 2013). Including a temperature error of ± 5 °C increases total propagated uncertainties to ± 300 ppmv (higher WMMT implies higher p_{CO2}). Such a low p_{CO2} (<750 ppmv) contrasts with marine proxies that typically imply values of 800–1000 ppmv

immediately preceding the EOT (Pearson et al., 2009; Zhang et al., 2013). A drop in p_{CO2} just before Oi-1, however, as implied by our data, is a logical driver of global cooling during the EOT (DeConto and Pollard, 2003).

5.3. Carbon isotopes and MAP

Specific MAP estimates from carbon isotopes (Fig. 5A) show no resolvable changes from 43 to 30 Ma, even across the EOT. A mean calculated value of ~450 mm/yr (±200 mm) implies semi-arid conditions. Systematic errors would shift all data uniformly, so the constancy of these estimates, which reflects the constant offset between tooth enamel and atmospheric $\delta^{13}C$ (Fig. 4C), is robust. Note that slightly higher apparent MAP values during the Barrancan (c. 600 mm/yr) are controlled by low $\delta^{13}C$ values during an ~200 ka interval (ellipse in Fig. 4A); omitting these data lowers Barrancan MAP to ~400 mm/yr, indistinguishable from the Vacan and Mustersan. During the early Deseadan (27.2 Ma), MAP appears to drop. However, we have relatively few fossils from this locality (Fig. 2B), so although their compositions are internally consistent, we are cautious in interpreting this time slice. They certainly do not indicate wetter conditions. MAP at ~23 and ~21 Ma shows a distinct rise. Paleofloral estimates of MAP in southern South America (Hinojosa, 2005; Hinojosa and Villagrán, 2005) are generally higher (average c. 1000 mm/yr), but uncertainties are large (standard errors on the order of 450–1000 mm), and minimum estimates overlap our calculations. A systematic calibration error of 200–250 mm/yr for isotope-derived MAP, which is within calibration uncertainties, would also help reconcile these datasets.

Paleosol estimates of MAP based on soil type and chemistry show generally high MAP (up to 1300 mm/yr) in the Koluel–Kaike Formation, and a drop towards low MAP values similar to ours at 43 Ma (Krause

et al., 2010). Lateritic soils, characteristic of the lower Koluel–Kaike Formation, form only at high MAP (≥1200 mm/yr; e.g. Retallack, 2008), strongly suggesting aridification from the (lower) Koluel–Kaike to the Vacan. In the Sarmiento Formation at Gran Barranca, estimates of MAP from paleosols (or the inferred vegetation associated with them; Bellosi and González, 2010) and carbon isotope measurements overlap, but suggest that the Barrancan may have been slightly wetter than times immediately before or after. Younger paleosols also suggest an increase in MAP after ~25 Ma. The higher MAP estimates from Bellosi and González (2010) for the Barrancan, late Deseadan and Colhuehuapian, however, correlate with more mature soils and lower sediment accumulation rates (by a factor of 2; Dunn et al., 2013). Paleosol-based MAP estimates may be systematically biased by different durations of paleosol development (Zanazzi et al., 2009). Although sedimentation rate might follow MAP (e.g., perhaps sediments accumulate faster during drier times because delivery rates increase), any factor that affects sedimentation rate could potentially masquerade as changes to MAP (e.g. perhaps sediments accumulate faster when ash production is higher). In that respect, indistinguishable floras in the late Barrancan and Mustersan (Fig. 3; Strömberg et al., 2013) may be more consistent with constant MAP than the decrease suggested by paleosols. Although early aridification and late wetting trends appear robust, the small variations between these trends may be less reliable. Overall, we view the data as more consistent with relatively constant MAP between 43 and at least 31 Ma, possibly as late as 25 Ma.

5.4. The paleoclimatic significance of high MAP floral indicators

The semi-arid conditions inferred from our record might at first appear at odds with MAP calculations and ecosystem reconstructions from leaf physiognomy and palynofloral and phytolith assemblages
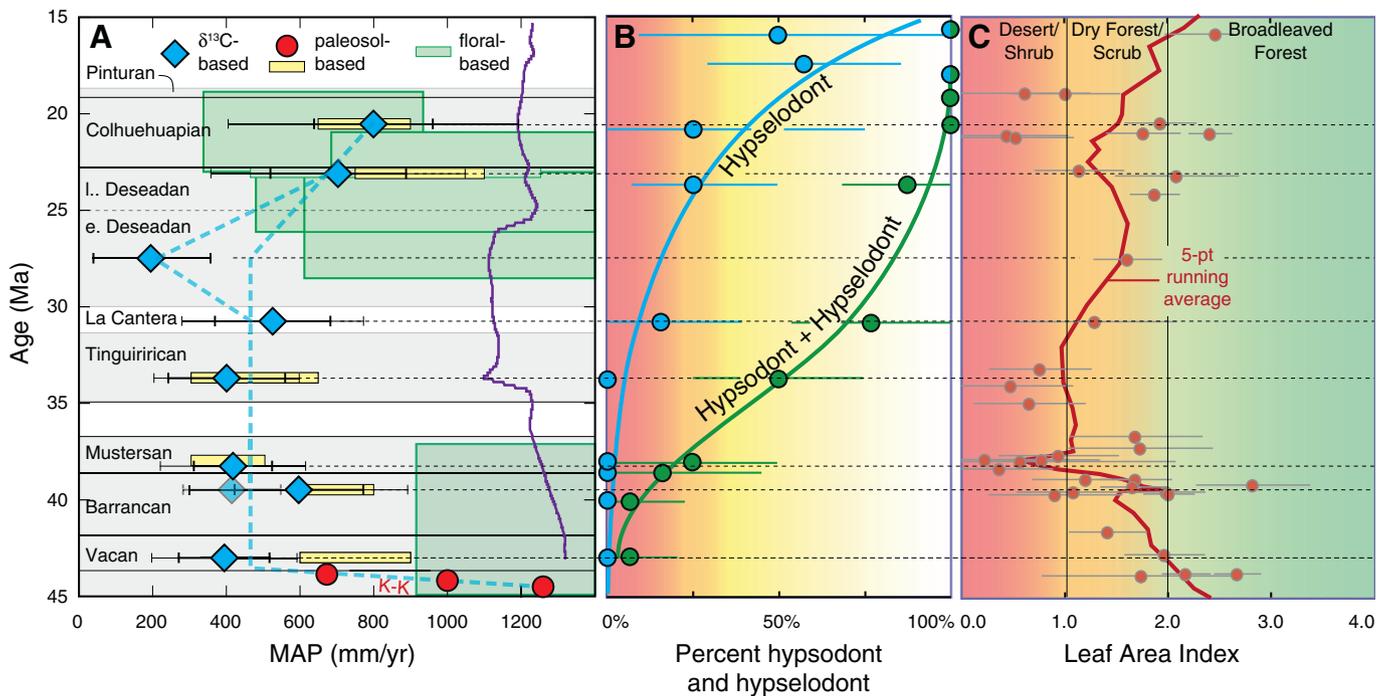

Fig. 5. (A) Estimate of mean annual precipitation (MAP) from tooth enamel $\delta^{13}C$ values (this study), paleosols (red, yellow symbols; Krause et al., 2010; Bellosi and González, 2010) and macrofloras (green bars; Hinojosa, 2005; Hinojosa and Villagrán, 2005; ages corrected in Dunn et al., 2015), implying aridification between ~48 and ~43 Ma, dry conditions until 25 Ma (possibly wetter at ~39 Ma), and an increase in MAP towards 20 Ma. Light symbol for Barrancan shows the effect of omitting a low $\delta^{13}C$ cluster in a specific horizon (ellipse, Fig. 4A). K–K = Koluel–Kaike Formation. Error bars are propagated 2s.e. in $\delta^{13}C$. (B) Notoungulate hypsodonty record for central Patagonia showing the gradual changes through time. Green dots show percent hypsodont plus hypselodont taxa; blue dots show hypselodont percentages only. Error bars are bootstrapped 95% confidence limits. (C) Leaf area index from Dunn et al. (2015) with approximate boundaries of major ecosystems, corroborating relatively dry (open) conditions from the late Barrancan and Mustersan (late Eocene) through middle Colhuehuapian (early Miocene). Red line is a 5-point running average; error bars are 95% confidence intervals. Dashed lines temporally correlate MAP estimates with hypsodonty and leaf area index records.

from southern South America. The high abundance of palms prior to the early Miocene and the occurrence of gingers in the middle Eocene, as well as the generally 'mixed' composition of the floras have commonly been assumed to reflect high MAP, c. 1000 mm/yr or more (Hinojosa, 2005; Hinojosa and Villagrán, 2005; Hinojosa et al., 2006; Barreda and Palazzesi, 2007; Quattrocchio et al., 2013; Strömberg et al., 2013). Several factors qualify inferences from floras, however. First, MAP estimates from leaf physiognomy carry large uncertainties – 40 to 65% – and the minimum bounds on MAP overlap our isotope-based estimates after accounting for age uncertainties (Fig. 5; Dunn et al., 2015). Second, the leaf physiognomy database has traditionally been heavily skewed towards northern hemisphere floras. Estimates of MAT show hemispheric bias, so temperature estimates now use hemisphere-specific calibrations (e.g. Hinojosa et al., 2011; Peppe et al., 2011; Kennedy et al., 2014). Similar hemispheric bias might occur for MAP, but is not yet studied. Third, although confined primarily to tropical rainforests today (e.g., Couvreur and Baker, 2013), palms contain wider ecological tolerance than is commonly recognized. Specifically, many members of the South American clade Attaleinae, which is represented by Paleocene fossils nearby (Futey et al., 2012), are relatively tolerant of water stress and disturbance. Thus, the commonly assumed correspondence between palms and high MAP may collapse in this region of South America — quantitative MAP estimates overlap semiarid conditions, and the palms that were present may have been relatively resistant to water stress. These observations do not explain gingers, but perhaps they were restricted to local wet depressions, which can occur in a variety of settings.

A final consideration is that plants close their stomata under higher p_{CO_2}, which dramatically improves water use efficiency (Ehleringer and Cerling, 1995; Ainsworth and Rogers, 2007; Ibrahim et al., 2010). For example, steadily increasing p_{CO_2} has measurably improved water use efficiency across Eurasia during the last century (but without changing isotope discrimination: Saurer et al., 2004). This effect has two implications in the context of higher p_{CO_2} during the Eocene and possibly later periods. First, plants such as palms that are now considered to be restricted to relative wet ecosystems could have thrived under drier conditions such as we propose here (Dunn et al., 2015). Second, because plants contribute significantly to atmospheric water vapor, improved water use efficiency would have diminished water vapor worldwide, slowing the water cycle and decreasing MAP. Overall, we appreciate the apparent disparity between our isotope-based estimates of MAP vs. taxonomic floral observations, but suggest that our estimates in the face of other factors are quantitatively correct and, in fact, hint at non-analog ecosystems in Earth's past.

5.5. Did Patagonian dust drive Eocene cooling and the Eocene–Oligocene Transition?

The EOT is generally understood to reflect marine and atmospheric circulation responses to the opening of marine gateways between Antarctica and both South America and Australia (Kennett, 1977), and is associated with an increase in southern ocean productivity, an increase in terrestrial sediment delivery to the southern ocean, and a decrease in p_{CO_2} (e.g., see Salamy and Zachos, 1999; Coxall and Wilson, 2011; Zhang et al., 2013). Here we propose that these environmental changes were all linked through Patagonian dust production as a result of the semi-arid climate reconstructed from isotopes and other lines of evidence (see above).

Some of the highest sustained winds on Earth blow across Patagonia between 40 and 50° S latitude – the so-called "Roaring 40s" – which together with unusually extensive exposures of highly erodable volcanic dust deposits help explain why Patagonia is the largest source of dust to the southern oceans during the Quaternary (Wolff et al., 2006; Li et al., 2008). We suggest that the output of dust from Patagonia has been substantial during at least the last 35 Ma. Progressive isolation of Antarctica and development of the Antarctic Circumpolar Current

during the Eocene and early Oligocene likely increased wind speeds across Patagonia (Ladant et al., 2014). If Patagonia was already relatively dry by the end of the Eocene (Mustersan, Fig. 5; Dunn et al., 2015), increased delivery of dust-sourced Fe, Si and P to southern oceans from this already dry and highly erodable environment (sparsely vegetated, tephric soils) would have promoted higher productivity, particularly of silicifiers (Diester-Haass and Zahn, 1996; Salamy and Zachos, 1999; Coxall et al., 2005) and decreased CO_2, much as increased dust delivery during the Pleistocene served as a positive feedback in reducing CO_2 and intensifying glaciations (e.g., Martin, 1990; Martinez-Garcia et al., 2011). The drawdown in CO_2 from the late Eocene to Oligocene (Zhang et al., 2013) served as a positive feedback to drive Antarctic glaciation and thermal isolation, ultimately transforming Earth from greenhouse to icehouse conditions. One notable feature of Eocene–Oligocene climate is the long decline in global temperature between 42 and 34 Ma (i.e. between the MECO and EOT; Zachos et al., 2001; Fig. 2) and in p_{CO_2} between 42 and ~25 Ma (Zhang et al., 2013). If aridification of Patagonia played a key role in this process, then global climate responded slowly overall, albeit with a marked step at the EOT. Further studies of mid-Cenozoic dust accumulation in South Atlantic marine cores would help test this hypothesis.

5.6. Faunal evolution: is the Court Jester a viable hypothesis?

Although Patagonian notoungulates crossed a hypsodonty index threshold of 1.0 relatively early (Strömberg et al., 2013), the overall record of increasing proportions of hypsodont and hypselodont taxa appears remarkably gradual (Figs. 2B, 5B). Indeed, if hypsodonty was an adaptation to dry, dusty environments, then it is striking that, although notoungulate hypsodonty did begin increasing soon after the initiation of semi-arid conditions by the late Eocene, the proportion of hyposodont + hypselodont taxa did not approach 100% for at least another 7 Ma, arguably until 20 Ma. Similarly, hypselodont taxa show a slow increase and do not constitute a majority in faunas even after ~20 Ma. The correspondence of reduced MAP, reduced vegetation cover, and increased hypsodonty does make sense — researchers have long recognized that lower MAP correlates with lower plant biomass, increased erosion, and increased sediment concentration in streams (Langbein and Schumm, 1958). Indeed modern day Patagonia is remarkable for its high wind speed and anomalously high rates of dust remobilization and deposition (Paruelo et al., 1998; Zender et al., 2003). Yet, the seemingly gradual increases in hypsodont + hypselodont taxa in the context of relatively constant climate and vegetation composition and structure appear inconsistent with the idea of a constant, directional environmental driver (Court Jester). Xenarthrans (especially sloths and armadillos) and rodents show changes in diversity and tooth morphology over the same time frame in the mid-Cenozoic that similarly cannot be explained by long-term changes in environment (Madden et al., 2010).

Despite this apparent lack of correlation between climatic and faunal patterns, we argue that it cannot be explained by the Red Queen hypothesis. The Red Queen is most relevant for asymmetric co-evolutionary relationships, such as that between predator and prey or parasite and host (Dawkins and Krebs, 1979; Vermeij and Roopnarine, 2013). Plants as herbivore "prey" are not directly responsible for the abrasiveness that is thought to have been the trigger for hypsodonty evolution in notoungulates (although it cannot be ruled out that plants evolved ways to capture more dust) (Strömberg et al., 2013; Dunn et al., 2015); furthermore, competition for limited plant resources among notoungulates is more likely to have led to intraspecific rather than interspecific competition (Dawkins and Krebs, 1979); in contrast, interaction among competing species is more likely to lead to niche divergence ("character displacement"; e.g., Brown and Wilson, 1956; Pritchard and Schluter, 2001).

If the physical environment drives faunal evolution (Court Jester), yet relatively dry ecosystems were already established by the late Eocene (Dunn et al., 2015; Fig. 5), why would hypsodonty evolve over
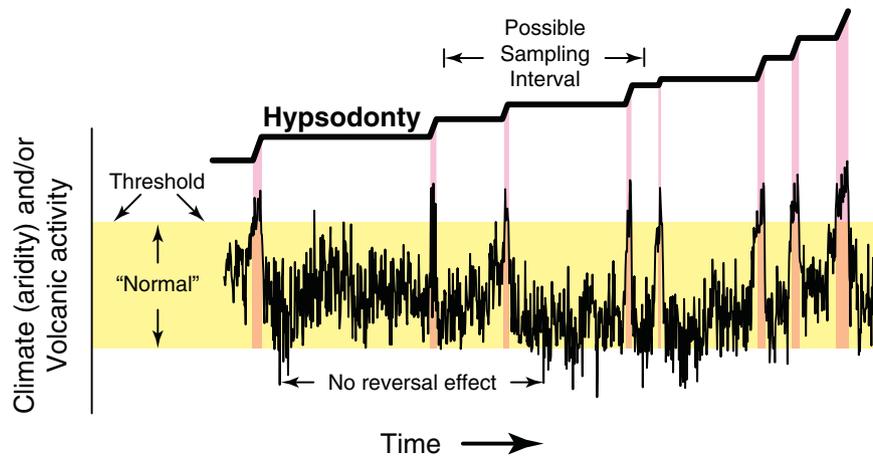
Fig. 6. Schematic illustration of Ratchet effect to explain progressive increases in hypsodonty index during quasi-static climate, volcanic activity, or both. Oscillations in physical conditions will occasionally induce brief periods of anomalously high aridity and/or volcanic activity (i.e. exceed a threshold), and hypsodonty will increase slightly as a result of natural selection. As long as there is no selection for decreased hypsodonty index during anomalously low aridity and/or volcanic activity ("no reversal effect"), hypsodonty will appear to increase smoothly.

tens of millions of years? The answer might be that the observed long-term changes in hypsodonty are the cumulative effect of many short-lived instances of directional natural selection. Research has shown that trait selection occurs on scales of tens to thousands of generations, which translates to hundreds to tens of thousands of years (e.g., Barrick and Lenski, 2013), not millions of years; thus, one possible modification to the Court Jester hypothesis invokes small-scale climatic events or other perturbations that occur on time-scales shorter than we can normally sample within otherwise stable conditions. Such a mechanism has been dubbed the "Ratchet" (West-Eberhard, 2003; Lister, 2004; Fig. 6). For example, climate oscillations on time-scales of ~20, ~40, ~100 and ~400 ka, which are all too short for us to resolve fully with our current data, may have induced brief periods of enhanced aridity (dustiness) that in turn induced selection events that led to slight increases in hypsodonty (Fig. 6) — in keeping with the notion that short term, externally triggered instances of directional selection dominate in adaptive evolution (Vermeij and Roopnarine, 2013). For example, the anomalously low δ^{13}C cluster in the Barrancan might represent the opposite — a brief (c. 200 ka) interval of enhanced precipitation. Similarly, an ~200 ka interval of reduced fire intensity and increased palm abundance has been inferred in the Vera member immediately after the EOT (Selkin et al., 2015). Such oscillations may be generally responsible for the variability observed in the records of phytolith assemblage composition and reconstructed Leaf Area Index (Strömberg et al., 2013; Dunn et al., 2015; Figs. 3, 5). Over many million years, these incremental changes could accumulate to produce the observed monotonic, quasi-continuous increase in hypsodonty (Figs. 5B, 6), much as has been proposed to explain evolution of hypsodonty and enamel complexity in proboscideans since the late Miocene in response to aridification and exploitation of developing grassland eco-systems (Lister, 2013). Another possible driver relates to dust delivery from volcanic sources. Brief intervals of relatively high volcanic activity and enhanced dustiness might have induced selection for increased hypsodonty that persisted and accumulated (Fig. 6). Changes to the physical environment would still have driven hypsodonty (Court Jester), but only during brief cycles that exceeded the mean climate normally sampled by our averaged data, the long-term volcanic state reflected in the large-scale sedimentary sequence, or both. As long as increased hypsodonty conferred no evolutionary disadvantage during less arid and/or less dusty cycles (i.e., no reversal effect: Fig. 6), there would be no selective advantage for reduced tooth crown height, resulting in morphological stasis (Vermeij and Roopnarine, 2013).

6. Conclusions

1) Oxygen isotopes of tooth enamel confirm minimal changes from 43 to 21 Ma (Kohn et al., 2004, 2010, this study), except for late Deseadan fossils possibly during the Mi1 glaciation at ~23 Ma. These data can be reconciled with a moderate temperature drop (3–4 °C) across the Eocene–Oligocene transition, and an additional ~4 °C drop during Mi1, although changes to moisture source are alternatively possible. Oxygen isotopes in fossil bone suggest a mean alteration temperature of ~16 °C, with no resolvable change from ~40 to ~20 Ma, including across the Eocene–Oligocene transition.

2) Pedogenic carbonate δ^{13}C values from the initial stages of the Eocene–Oligocene climatic transition imply lower p_{CO2} (430 ± 300 ppmv) than estimated from marine proxies (800–1000 ppmv).

3) Our isotope-based estimates of mean annual precipitation combined with previous work on paleosols indicate relatively wet but aridifying conditions at ~45 Ma, and dry conditions (MAP ~450 mm/yr) from 43 to at least 31 Ma, with a possible drop in MAP at 27.2 Ma. MAP increased to ~800 mm/yr by 20 Ma. A relatively static climate between ~43 and ~20 Ma is consistent with relatively constant floral compositions (Strömberg et al., 2013) and reconstructed Leaf Area Indices (Dunn et al., 2015).

4) A dry Patagonia during the Eocene and Oligocene may have served as a positive feedback to protracted global cooling and decreased p_{CO2} via production and delivery of dust to Southern Ocean, promoting enhanced productivity, particularly of silicifiers (e.g., Diester-Haass and Zahn, 1996; Coxall et al., 2005) and drawdown of atmospheric CO_2 (Zhang et al., 2013).

5) If hypsodonty is an adaptation to dust and aridity (e.g., Fortelius et al., 2002; Damuth and Janis, 2011), then it evolved relatively slowly among Patagonian notoungulates, spanning over 20 Ma after the initiation of dry environments. Such protracted evolution may be explained by the Ratchet evolution model, in which small oscillations in the physical environment, for example from variations in climate or upwind volcanic activity, within an otherwise relatively static environment drive small morphological shifts that accumulate over time.

Ratchet model. Funded by NSF grants EAR0842367 for instrumentation, EAR0819837 and EAR1349749 to MJK, DEB1110354 to RED and CAES, EAR0819910 to CAES, EAR0819842 to RHM, a FONCyT grant to AAC, and the LSAMP program at BSU.

Appendix A. Supplementary data

Supplementary data to this article can be found online at http://dx.doi.org/10.1016/j.palaeo.2015.05.028.

References

Ainsworth, E.A., Rogers, A., 2007. The response of photosynthesis and stomatal conductance to rising [CO_2]: mechanisms and environmental interactions. Plant Cell Environ. 30, 258–270.

Alroy, J., Koch, P.L., Zachos, J.C., 2000. Global climate change and North American mammalian evolution. Paleobiology 26, 259–288.

Barnosky, A.D., 2001. Distinguishing the effects of the red queen and court jester on Miocene mammal evolution in the northern Rocky Mountains. J. Vertebr. Paleontol. 21, 172–185.

Barnosky, A.D., Hadly, E.A., Bell, C.J., 2003. Mammalian response to global warming on varied temporal scales. J. Mammal. 84, 354–368.

Barreda, V., Palazzesi, L., 2007. Patagonian vegetation turnovers during the Paleogene–Early Neogene: origin of arid-adapted floras. Bot. Rev. 73, 31–50.

Barrick, J.E., Lenski, R.E., 2013. Genome dynamics during experimental evolution. Nat. Rev. Genet. 14, 827–839.

Bell, G., 1982. The Masterpiece of Nature: The Evolution and Genetics of Sexuality. University of California Press, Berkeley (635 pp.).

Bellosi, E.S., 2010. Physical stratigraphy of the Sarmiento Formation (Middle Eocene–Lower Miocene) at Gran Barranca, central Patagonia. In: Madden, R.H., Carlini, A.A., Vucetich, M.G., Kay, R.F. (Eds.), The Paleontology of Gran Barranca: Evolution and Environmental Change Through the Middle Cenozoic of Patagonia. Cambridge University Press, Cambridge, UK, pp. 19–31.

Bellosi, E.S., González, M.G., 2010. Paleosols of the middle Cenozoic Sarmiento Formation, central Patagonia. In: Madden, R.H., Carlini, A.A., Vucetich, M.G., Kay, R. (Eds.), The Paleontology of Gran Barranca: Evolution and Environmental Change Through the Middle Cenozoic of Patagonia. Cambridge University Press, Cambridge, UK, pp. 293–305.

Bowling, D.R., Pataki, D.E., Randerson, J.T., 2008. Carbon isotopes in terrestrial ecosystem pools and CO_2 fluxes. New Phytol. 178, 24–40.

Breecker, D.O., Sharp, Z.D., McFadden, L.D., 2009. Seasonal bias in the formation and stable isotopic composition of pedogenic carbonate in modern soils from central New Mexico, USA. Geol. Soc. Am. Bull. 121, 630–640.

Breecker, D.O., Sharp, Z.D., MacFadden, B.J., 2010. Atmospheric CO_2 concentrations during ancient greenhouse climates were similar to those predicted for A.D. 2100. Proc. Natl. Acad. Sci. U. S. A. 107, 576–580.

Brown Jr., W.L., Wilson, E.O., 1956. Character displacement. Syst. Zool. 5, 49–64.

Buckley, M., 2015. Ancient collagen reveals evolutionary history of the endemic South American 'ungulates'. Proc. R. Soc. B Biol. Sci. 282. http://dx.doi.org/10.1098/rspb.2014.2671.

Cassini, G.H., Cardeño, E., Villafañe, A.L., Muñoz, N.A., 2012. Paleobiology of Santacrucian native ungulates (Meridiungulata: Astrapotheria, Litopterna and Notoungulata). In: Vizcaíno, S., Kay, R.F., Bargo, M. (Eds.), Early Miocene Paleobiology in Patagonia: High-latitude Paleocommunities of the Santa Cruz Formation. Cambridge University Press, Cambridge, UK, pp. 243–286.

Cerling, T.E., 1991. Carbon dioxide in the atmosphere: evidence from Cenozoic and Mesozoic paleosols. Am. J. Sci. 291, 377–400.

Cerling, T.E., 1999. In: Thiry, M., Simon-Coincon, R. (Eds.), Stable Isotopes in Paleosol Carbonates. Palaeoweathering, Palaeosurfaces, and Related Continental Deposits 27. International Association of Sedimentologists Special Publication, Oxford, pp. 43–60.

Cerling, T.E., Harris, J.M., 1999. Carbon isotope fractionation between diet and bioapatite in ungulate mammals and implications for ecological and paleoecological studies. Oecologia 120, 347–363.

Cerling, T.E., Harris, J.M., MacFadden, B.J., Leakey, M.G., Quade, J., Eisenmann, V., Ehleringer, J.R., 1997. Global vegetation change through the Miocene/Pliocene boundary. Nature 389 (6647), 153–158.

Cifelli, R.L., 1985. Biostratigraphy of the Casamayoran, early Eocene, of Patagonia. Am. Mus. Novit. 2820, 1–16.

Cotton, J.M., Sheldon, N.D., 2012. New constraints on using paleosols to reconstruct atmospheric p_{CO2}. Geol. Soc. Am. Bull. 124, 1411–1423.

Couvreur, T.L.P., Baker, W.J., 2013. Tropical rain forest evolution: palms as a model group. BioMed Central 11, 1–4.

Coxall, H.K., Wilson, P.A., 2011. Early Oligocene glaciation and productivity in the eastern equatorial Pacific: insights into global carbon cycling. Paleoceanography 26. http://dx.doi.org/10.1029/2010PA002021.

Coxall, H.K., Wilson, P.A., Palike, H., Lear, C.H., Backman, J., 2005. Rapid stepwise onset of Antarctic glaciation and deeper calcite compensation in the Pacific Ocean. Nature 433, 53–57.

Croft, D.A., 2001. Cenozoic environmental change in South America as indicated by mammalian body size distributions (cenograms). Divers. Distrib. 7, 271–287.

Damuth, J., Janis, C.M., 2011. On the relationship between hypsodonty and feeding ecology in ungulate mammals, and its utility in palaeoecology. Biol. Rev. 86, 733–758.

Dawkins, R., Krebs, J.R., 1979. Arms races between and within species. Proc. R. Soc. Lond. B Biol. Sci. 205, 489–511.

DeConto, R.J., Pollard, D., 2003. Rapid Cenozoic glaciation of Antarctica triggered by declining atmospheric CO_2. Nature 421, 245–249.

Diester-Haass, L., Zahn, R., 1996. Eocene–Oligocene transition in the Southern Ocean: history of water mass circulation and biological productivity. Geology 24, 163–166.

Douglas, P.M.J., Affek, H.P., Ivany, L.C., Houben, A.J.P., Sijp, W.P., Sluijs, S., Schouten, S., Pagani, M., 2014. Pronounced zonal heterogeneity in Eocene southern high-latitude sea surface temperatures. Proc. Natl. Acad. Sci. U. S. A. 111, 6582–6587.

Dunn, R.E., Madden, R.H., Kohn, M.J., Schmitz, M.D., Strömberg, C.A.E., Carlini, A.A., Ré, G.H., Crowley, J., 2013. A new chronology for middle Eocene–early Miocene South American Land Mammal Ages. Geol. Soc. Am. Bull. 125, 539–555.

Dunn, R.E., Strömberg, C.A.E., Madden, R.H., Kohn, M.J., Carlini, A.A., 2015. Linked canopy, climate and faunal change in the Cenozoic of Patagonia. Science 347, 258–261.

Edwards, E.J., Osborne, C.P., Strömberg, C.A.E., Smith, S.A., C_4 Grasses Consortium, 2010. The origins of C_4 grasslands: integrating evolutionary and ecosystem science. Science 328, 587–591.

Ehleringer, J.R., Cerling, T.E., 1995. Atmospheric CO_2 and the ratio of intercellular to ambient CO_2 concentrations in plants. Tree Physiol. 15, 105–111.

Ekart, D.D., Cerling, T.E., Montanez, I.P., Tabor, N.J., 1999. A 400 million year carbon isotope record of pedogenic carbonate: implications for paleoatmospheric carbon dioxide. Am. J. Sci. 299 (10), 805–827.

Figueirido, B., Janis, C.M., Pérez-Claros, J.A., De Renzi, M., Palmqvist, P., 2012. Cenozoic climate change influences mammalian evolutionary dynamics. Proc. Natl. Acad. Sci. 109, 722–727.

Finarelli, J.A., Badgley, C., 2010. Diversity dynamics of Miocene mammals in relation to the history of tectonism and climate. Proc. R. Soc. B Biol. Sci. 277, 2721–2726.

Fletcher, T.M., Janis, C.M., Rayfield, E.J., 2010. Finite element analysis of ungulate jaws: can mode of digestive physiology be determined. Palaeontol. Electron. 10 (3).

Fortelius, M., Eronen, J., Jernvall, J., Liu, L., Pushkina, D., Rinne, J., Tesakov, A., Vislobokova, I., Zhang, Z., Zhou, L., 2002. Fossil mammals resolve regional patterns of Eurasian climate change over 20 million years. Evol. Ecol. Res. 4, 1005–1016.

Fricke, H.C., O'Neil, J.R., 1996. Inter- and intra-tooth variation in the oxygen isotope composition of mammalian tooth enamel phosphate; implications for palaeoclimatological and palaeobiological research. Palaeogeogr. Palaeoclimatol. Palaeoecol. 126, 91–99.

Futey, M.K., Gandolfo, M.A., Zamaloa, M.C., Cuneo, R., Cladera, G., 2012. Arecaceae fossil fruits from the Paleocene of Patagonia, Argentina. Bot. Rev. 78, 205–234.

Hinojosa, L.F., 2005. Cambios climáticos y vegetacionales inferidos a partir de paleofloras cenozoicas del sur de Sudamérica. Rev. Geol. Chile 32, 95–115.

Hinojosa, L.F., Villagrán, C., 2005. Did South American mixed paleofloras evolve under thermal equability of in the absence of an effective Andean barrier during the Cenozoic? Palaeogeogr. Palaeoclimatol. Palaeoecol. 217, 1–23.

Hinojosa, L.F., Armesto, J.J., Villagrán, C., 2006. Are Chilean coastal forests pre-Pleistocene relicts? Evidence from foliar physiognomy, palaeoclimate, and phytogeography. J. Biogeogr. 33, 331–341.

Hinojosa, L.F., Pérez, F., Gaxiola, A., Sandoval, I., 2011. Historical and phylogenetic constraints on the incidence of entire leaf margins: insights from a new South American model. Glob. Ecol. Biogeogr. 20, 380–390.

Ibrahim, M.H., Jaafar, H.Z.E., Harun, M.H., Yusop, M.R., 2010. Changes in growth and photosynthetic patterns of oil palm (*Elaeis guineensis* Jacq.) seedlings exposed to short-term CO_2 enrichment in a closed top chamber. Acta Physiol. Plant. 32, 305–313.

Jacobs, B.F., Kingston, J.D., Jacobs, L.L., 1999. The origin of grass-dominated ecosystems. Ann. Mo. Bot. Gard. 86, 590–643.

Kaiser, T.M., Müller, D.W.H., Fortelius, M., Schulz, E., Codron, D., Clauss, M., 2013. Hypsodonty and tooth facet development in relation to diet and habitat in herbivorous ungulates: implications for understanding tooth wear. Mammal Rev. 43, 34–46.

Kay, R.F., Madden, R.H., Vucetich, M.G., Carlini, A.A., Mazzoni, M.M., Ré, G.H., Heizler, M., Sandeman, H., 1999. Revised geochronology of the Casamayoran South American Land Mammal Age: climatic and biotic implications. Proc. Natl. Acad. Sci. 96, 13235–13240.

Kennedy, E.M., Arens, N.C., Reichgelt, T., Spicer, R.A., Spicer, T.E.V., Stranks, L., Yang, J., 2014. Deriving temperature estimates from Southern Hemisphere leaves. Palaeogeogr. Palaeoclimatol. Palaeoecol. 412, 80–90.

Kennett, J.P., 1977. Cenozoic evolution of Antarctic glaciation, the circum-Antarctic Ocean, and their impact on global paleoceanography. J. Geophys. Res. 82, 3843–3860.

Kim, S.-T., O'Neil, J.R., 1997. Equilibrium and nonequilibrium oxygen isotope effects in synthetic carbonates. Geochim. Cosmochim. Acta 61, 3461–3475.

Koch, P.L., Tuross, N., Fogel, M.L., 1997. The effects of sample treatment and diagenesis on the isotopic integrity of carbonate in biogenic hydroxylapatite. J. Archaeol. Sci. 24, 417–429.

Kohn, M.J., 1996. Predicting animal $\delta^{18}O$: accounting for diet and physiological adaptation. Geochim. Cosmochim. Acta 60, 4811–4829.

Kohn, M., 2010. Carbon isotope compositions of terrestrial C3 plants as indicators of (paleo)ecology and (paleo)climate. Proc. Natl. Acad. Sci. 107, 19691–19695.

Kohn, M.J., 2014. No correction of terrestrial C3-plant carbon isotope compositions for p_{CO2}. Paleontol. Soc. Spec. Publ. 13, 42.

Kohn, M.J., Cerling, T.E., 2002. Stable isotope compositions of biological apatite. Rev. Mineral. Geochem. 48, 455–488.

Kohn, M.J., Dettman, D.L., 2007. Paleoaltimetry from stable isotope compositions of fossils. Rev. Mineral. Geochem. 66, 119–154.

Kohn, M.J., Fremd, T.J., 2007. Tectonic controls on isotope compositions and species diversification, John Day Basin, central Oregon. PaleoBios 27, 48–61.

Kohn, M.J., Law, J.M., 2006. Stable isotope chemistry of fossil bone as a new paleoclimate indicator. Geochim. Cosmochim. Acta 70, 931–946.

Kohn, M.J., McKay, M.P., 2012. Paleoecology of late Pleistocene–Holocene faunas of eastern and central Wyoming, USA, with implications for LGM climate models. Palaeogeogr. Palaeoclimatol. Palaeoecol. 326–328, 42–53.

Kohn, M.J., Miselis, J.L., Fremd, T.J., 2002. Oxygen isotope evidence for progressive uplift of the Cascade Range, Oregon. Earth Planet. Sci. Lett. 204, 151–165.

Kohn, M.J., Josef, J.A., Madden, R.H., Kay, R., Vucetich, G., Carlini, A.A., 2004. Climate stability across the Eocene–Oligocene transition, southern Argentina. Geology 32, 621–624.

Kohn, M.J., Zanazzi, A., Josef, J.A., 2010. Stable isotopes of fossil teeth and bones at Gran Barranca as a monitor of climate change and tectonics. In: Madden, R.H., Carlini, A.A., Vucetich, G.M., Kay, R.F. (Eds.), The Paleontology of Gran Barranca: Evolution and Environmental Change Through the Middle Cenozoic of Patagonia. Cambridge University Press, Cambridge, pp. 341–361.

Kovalevsky, V.O., 1874. Monographie der Gattung Anthracotherium Civ., und Versuch einer natürlichen Classification der fossilen Huftiere. Palaeontographica 22, 210–285.

Krause, J.M., Bellosi, E.S., Raigemborn, M.S., 2010. Lateritized tephric palaeosols from Central Patagonia, Argentina: a southern high-latitude archive of Palaeogene global greenhouse conditions. Sedimentology 57, 1721–1749.

Ladant, J.-B., Donnadieu, Y., Dumas, C., 2014. Links between CO_2, glaciation and water flow: reconciling the Cenozoic history of the Antarctic Circumpolar Current. Clim. Past Discuss. 10, 2397–2416.

Langbein, W.B., Schumm, S.A., 1958. Yield of sediment in relation to mean annual precipitation. Trans. Am. Geophys. Union 39, 1076–1084.

Lawver, L.A., Dalziel, I.W.D., Gahagan, L.M., 2015. Intercontinental migration routes for South American land mammals: paleogeographic constraints. In: Rosenberger, A.L., Tejedor, M.F. (Eds.), Origins and Evolution of Cenozoic South American Mammals. Springer, Berlin.

Leopold, E., Denton, M., 1987. Comparative age of grassland and steppe east and west of the Northern Rocky Mountains. Ann. Mo. Bot. Gard. 74, 841–867.

Li, F., Ginoux, P., Ramaswamy, V., 2008. Distribution, transport, and deposition of mineral dust in the Southern Ocean and Antarctica: contribution of major sources. J. Geophys. Res. 113. http://dx.doi.org/10.1029/2007JD009190.

Lister, A.M., 2004. The impact of Quaternary Ice Ages on mammalian evolution. Philos. Trans. R. Soc. Lond. B 359, 221–241.

Lister, A.M., 2013. The role of behaviour in adaptive morphological evolution of African proboscideans. Nature 500, 331–334.

Madden, R.H., 2014. Hypsodonty in Mammals: Evolution, Geomorphology and the Role of Earth Surface Processes. Cambridge University Press, Cambridge (448 pp.).

Madden, R., Vucetich, G., Carlini, A.A., Kay, R., 2010. The Paleontology of Gran Barranca: Evolution and Environmental Change Through the Middle Cenozoic of Patagonia. Cambridge University Press, Cambridge, UK.

Martin, J.H., 1990. Glacial–interglacial CO_2 change: the iron hypothesis. Paleoceanography 5, 1–13.

Martinez-Garcia, A., Rosell-Melé, A., Jaccard, S.L., Geibert, W., Sigman, D.M., Haug, G.H., 2011. Southern Ocean dust–climate coupling over the past four million years. Nature 476, 312–316.

McNab, B.K., 2002. The physiological ecology of vertebrates. A View From Energetics. Cornell University Press, Ithaca, NY (576 pp.).

Miller, K.G., Wright, J.D., Fairbanks, R.G., 1991. Unlocking the ice house: Oligocene–Miocene oxygen isotopes, eustasy, and margin erosion. J. Geophys. Res. 96, 6829–6848.

Moreno, P.I., Villa-Martinez, R., Cardenas, M.L., Sagredo, E.A., 2012. Deglacial changes of the southern margin of the southern westerly winds revealed by terrestrial records from SW Patagonia (52 degrees S). Quat. Sci. Rev. 41, 1–21.

Palazzesi, L., Barreda, V., 2012. Fossil pollen records reveal a late rise of open-habitat ecosystems in Patagonia. Nat. Commun. http://dx.doi.org/10.1038/ncomms2299.

Paruelo, J.M., Beltrán, A., Jobbágy, E., Sala, O.E., Golluscio, R.A., 1998. The climate of Patagonia: general patterns and controls on biotic processes. Ecol. Aust. 8, 85–101.

Pearson, P.N., Foster, G.L., Wade, B.S., 2009. Atmospheric carbon dioxide through the Eocene–Oligocene climate transition. Nature 461, 1110–1113.

Pekar, S.F., DeConto, R.M., Harwood, D.M., 2006. Resolving a late Oligocene conundrum: deep-sea warming and Antarctic glaciation. Palaeogeogr. Palaeoclimatol. Palaeoecol. 231, 29–40.

Peppe, D.J., Royer, D.L., Cariglino, B., Oliver, S.Y., Newman, S., Leight, E., Enikolopov, G., Fernandez-Burgos, M., Herrera, F., Adams, J.M., Correa, E., Currano, E.D., Erickson, J.M., Hinojosa, L.F., Hoganson, J.W., Iglesias, A., Jaramillo, C.A., Johnson, K.R., Jordan, G.J., Kraft, N.J.B., Lovelock, E.C., Lusk, C.H., Niinemets, Ü., Peñuelas, J., Rapson, G., Wing, S.L., Wright, I.J., 2011. Sensitivity of leaf size and shape to climate: global patterns and paleoclimatic applications. New Phytol. 190, 724–739.

Pritchard, J.R., Schluter, D., 2001. Declining interspecific competition during character displacement: summoning the ghost of competition past. Evol. Ecol. Res. 3, 209–220.

Prothero, D.R., 1999. Does climatic change drive mammalian evolution? GSA Today 9, 1–5.

Prothero, D.R., 2004. Did impacts, volcanic eruptions, or climate change affect mammalian evolution? Palaeogeogr. Palaeoclimatol. Palaeoecol. 214, 283–294.

Quattrocchio, M.E., Martínez, M.A., Hinojosa, L.F., Jaramillo, C., 2013. Quantitative analysis of Cenozoic palynofloras from Patagonia, southern South America. Palynology 37, 246–258.

Ré, G.H., Geuna, S., Vilas, J.F., 2010a. Paleomagnetism and magnetostratigraphy of the Sarmiento Formation (Eocene–Miocene) at Gran Barranca, Chubut, Argentina. In: Madden, R., Carlini, A.A., Vucetich, M.G., Kay, R.F. (Eds.), The Paleontology of Gran Barranca: Evolution and Environmental Change Through the Middle Cenozoic of Patagonia. Cambridge University Press, Cambridge, UK, pp. 32–45.

Ré, G., Bellosi, E.S., Heizler, M., Vilas, J., Madden, R.H., Carlini, A.A., Kay, R.F., 2010b. A geochronology of the Sarmiento Formation at Gran Barranca. In: Madden, R.H., Carlini, A.A., Vucetich, M.G., Kay, R. (Eds.), The Paleontology of Gran Barranca: Evolution and Environmental Change Through the Middle Cenozoic of Patagonia. Cambridge University Press, Cambridge, pp. 46–59.

Retallack, G.J., 2008. Cool-climate or warm-spike lateritic bauxites at high latitudes? J. Geol. 116, 558–570.

Romanek, C.S., Grossman, E.L., Morse, J.W., 1992. Carbon isotopic fractionation in synthetic aragonite and calcite; effects of temperature and precipitation rate. Geochim. Cosmochim. Acta 56, 419–430.

Salamy, K.A., Zachos, J.C., 1999. Latest Eocene–early Oligocene climate change and Southern Ocean fertility; inferences from sediment accumulation and stable isotope data. Palaeogeogr. Palaeoclimatol. Palaeoecol. 145, 61–77.

Sanson, G.D., Kerr, S.A., Gross, K.A., 2007. Do silica phytoliths really wear mammalian teeth? J. Archaeol. Sci. 34, 526–531.

Saurer, M., Siegwolf, R.T.W., Schweingruber, F.H., 2004. Carbon isotope discrimination indicates improving water-use efficiency of trees in northern Eurasia over the last 100 years. Glob. Chang. Biol. 10, 2109–2120.

Schubert, B.A., Jahren, A.H., 2012. Effect of atmospheric CO_2 concentration on carbon isotope fraction in C_3 land plants. Geochim. Cosmochim. Acta 96, 29–43.

Scott, W.B., 1937. A History of Land Mammals in the Western Hemisphere. MacMillan and Co., New York (286 pp.).

Selkin, P.A., Strömberg, C.A.E., Dunn, R.E., Kohn, M.J., Carlini, A.A., Davies-Vollum, K.S., Madden, R.H., 2015. Climate, dust, and fire across the Eocene–Oligocene transition, Patagonia. Geology (in press).

Sheldon, N.D., Tabor, N.J., 2009. Quantitative paleoenvironmental and paleoclimatic reconstruction using paleosols. Earth Sci. Rev. 95, 1–52.

Sheldon, N.D., Costa, E., Cabrera, L., Garces, M., 2012. Continental climatic and weathering response to the Eocene–Oligocene transition. J. Geol. 120 (2), 227–236.

Simpson, G.G., 1980. Splendid Isolation: The Curious History of South American Mammals. Yale University Press, New Haven (266 pp.).

Soil Survey Staff, 2010. Keys to Soil Taxonomy. 11th ed. USDA—Natural Resources Conservation Service, Washington, DC.

Spalletti, L., Mazzoni, M.M., 1979. Estratigrafia de la Formacion Sarmiento en la barranca sur del Lago Colhue-Huapi, provincia del Chubut. Rev. Asoc. Geol. Argent. 34, 271–281.

Srivastava, P., Patel, S., Singh, N., Jamir, T., Kumar, N., Artche, M., Patel, R.C., 2013. Early Oligocene paleosols of the Dagshai Formation, India: a record of the oldest tropical weathering in the Himalayan foreland. Sediment. Geol. 294, 142–156.

Stebbins, G.L., 1981. Coevolution of grasses and herbivores. Ann. Mo. Bot. Gard. 68, 75–86.

Stewart, G.R., Turnbull, M.H., Schmidt, S., Erskine, P.D., 1995. ^{13}C natural abundance in plant communities along a rainfall gradient: a biological integrator of water availability. Aust. J. Plant Physiol. 22, 51–55.

Strömberg, C.A.E., 2005. Decoupled taxonomic radiation and ecological expansion of open-habitat grasses in the Cenozoic of North America. Proc. Natl. Acad. Sci. 102, 11980–11984.

Strömberg, C.A.E., 2006. Evolution of hypsodonty in equids: testing a hypothesis of adaptation. Paleobiology 32, 236–258.

Strömberg, C.A.E., 2011. Evolution of grasses and grassland ecosystems. Annu. Rev. Earth Planet. Sci. 39, 517–544.

Strömberg, C.A.E., Werdelin, L., Friis, E.M., Sarac, G., 2007. The spread of grass-dominated habitats in Turkey and surrounding areas during the Cenozoic: phytolith evidence. Palaeogeogr. Palaeoclimatol. Palaeoecol. 250, 18–49.

Strömberg, C.A.E., Dunn, R.E., Madden, R.H., Kohn, M., Carlini, A.A., 2013. Decoupling the spread of grasslands from the evolution of grazer-type herbivores in South America. Nat. Commun. 4. http://dx.doi.org/10.1038/ncomms2508.

Tipple, B.J., Meyers, S.R., Pagani, M., 2010. The carbon isotope ratio of Cenozoic CO_2: a comparative evaluation of available geochemical proxies. Paleoceanography 25. http://dx.doi.org/10.1029/2009PA001851.

Van Valen, J.C., 1973. A new evolutionary law. Evol. Theory 1, 1–30.

Vermeij, G.J., Roopnarine, P.D., 2013. Reining in the Red Queen: the dynamics of adaptation and extinction reexamined. Paleobiology 39, 560–575.

Vucetich, M., Pérez, M., Ciancio, M., Carlini, A., Madden, R., Kohn, M., 2014. A new acaremyid rodent (Caviomorpha, Octodontoidea) from Scarritt Pocket, Deseadan (late Oligocene) of Patagonia (Argentina). J. Vertebr. Paleontol. 34, 689–698.

Webb, S.D., 1977. A history of savanna vertebrates in the New World. Part I: North America. Annu. Rev. Ecol. Syst. 8, 355–380.

Webb, S.D., 1978. A history of savanna vertebrates in the New World. Part II: South America and the Great Interchange. Annu. Rev. Ecol. Syst. 9, 393–426.

Welker, F., Collins, M.J., Thomas, J.A., Wadsley, M., Brace, S., Cappellini, E., Turvey, S.T., Reguero, M., Gelfo, J.N., Kramarz, A., Burger, J., Thomas-Oates, J., Ashford, D.A., Ashton, P.D., Rowsell, K., Porter, D.M., Kessler, B., Fischer, R., Baessmann, C., Kaspar, S., Olsen, J.V., Kiley, P., Elliott, J.A., Kelstrup, C.D., Mullin, V., Hofreiter, M., Willerslev, E., Hublin, J.-J., Orlando, L., Barnes, I., MacPhee, R.D.E., 2015. Ancient proteins resolve the evolutionary history of Darwin's South American ungulates. Nature. http://dx.doi.org/10.1038/nature14249.

West-Eberhard, M.J., 2003. Developmental Plasticity and Evolution. Oxford University Press, New York.

Wilf, P., Cúneo, R., Escapa, I.H., Pol, C., Woodburne, M.O., 2013. Splendid and seldom isolated: the paleobiogeography of Patagonia. Annu. Rev. Earth Planet. Sci. 41, 561–603.

Williams, S.H., Kay, R.F., 2001. A comparative test of adaptive explanations for hypsodonty in ungulates and rodents. J. Mamm. Evol. 8, 207–229.

Wolff, E.W., Fisher, H., Fundel, F., Ruth, U., Twarloh, B., Littot, G.C., Mulvaney, R., Röthlisberger, R., de Angelis, M., Boutron, C.F., Hansson, M., Jonsell, U., Hutterli, M.A., Lambert, F., Kaufmann, P., Stauffer, B., Stocker, T.F., Steffensen, J.P., Bigler, M., Siggaard-Andersen, M.L., Udisti, R., Becagli, S., Castellano, E., Severi, M., Wagenbach, D., Barbante, C., Gabrielli, P., Gaspari, B., 2006. Southern Ocean sea-ice extent, productivity and iron flux over the past eight glacial cycles. Nature 440, 491–494.

Woodburne, M.O., 2010. The Great American Biotic Interchange: dispersals, tectonics, climate, sea level and holding pens. J. Mamm. Evol. 17, 245–264.

Woodburne, M.O., Goin, F.J., Bond, M., Carlini, A.A., Gelfo, J.N., López, G.J., Iglesias, A., Zimicz, A.N., 2014. Paleogene land mammal faunas of South America; a response to global climatic changes and indigenous floral diversity. J. Mamm. Evol. 21, 1–73.

Zachos, J., Pagani, M., Sloan, L., Thomas, E., Billups, K., 2001. Trends, rhythms, and aberrations in global climate 65 Ma to present. Science 292, 686–693.

Zanazzi, A., Kohn, M.J., 2008. Ecology and physiology of White River mammals based on stable isotope ratios of teeth. Palaeogeogr. Palaeoclimatol. Palaeoecol. 257, 22–37.

Zanazzi, A., Kohn, M.J., MacFadden, B.J., Terry Jr., D.O., 2007. Large temperature drop across the Eocene–Oligocene transition in central North America. Nature 445, 639–642.

Zanazzi, A., Kohn, M.J., Terry Jr., D.O., 2009. Biostratigraphy and paleoclimatology of the Eocene–Oligocene boundary section at Toadstool Park, northwestern Nebraska, USA. Geol. Soc. Am. Spec. Pap. 452, 197–214.

Zender, C.S., Bian, H., Newman, D., 2003. Mineral dust entrainment and deposition (DEAD) model: description and 1990s dust climatology. J. Geophys. Res. 108. http://dx.doi.org/10.1029/2002JD002775.

Zhang, Y.G., Pagani, M., Liu, Z., Bohaty, S.M., DeConto, R.M., 2013. A 40-million-year history of atmospheric CO_2. Philos. Trans. R. Soc. Lond. A 371. http://dx.doi.org/10.1098/rsta.2013.0096.